



CLIMATE RISK ASSESSMENT

Ethiopia

APRIL 2025

Authors Dominick Dusseau^a, Abigail Lute^a, Abay Ezra^b, Jamie Cummings^a, Andrew Condia^a, Abigail Fennelly^a, Kelly Gassert^a, Carlos Dobler-Morales^a, Patrick Fedor^a, David McGlinchey^a, Christopher Schwalm^a

Contributors Ethiopian Ministry of Planning and Development, Ethiopian Ministry of Water and Energy, Ethiopian Disaster Risk Management Commission, Ethiopian Space Science and Geospatial Institute, Addis Ababa University

For more information about this analysis, or Woodwell's other climate risk assessments, please contact us at policy@woodwellclimate.org.

To learn more about Woodwell, please visit our website at woodwellclimate.org.



Who we are

^a **Woodwell Climate Research Center**

Woodwell Climate Research Center conducts scientific research to find solutions at the intersection of climate, people and nature. We work in partnership with leaders and communities to make a fair and meaningful impact on the climate crisis. Our scientists helped launch the United Nations Framework Convention on Climate Change in 1992 and, in 2007, Woodwell Climate scientists shared the Nobel Prize awarded to the Intergovernmental Panel on Climate Change. For 40 years, Woodwell Climate has combined practical experience and political impact to identify and support society-wide solutions that can be implemented immediately. This includes working with communities on the front line of the climate crisis.

^b **Woodwell Contractor, Ethiopian National, and Tufts University Postdoctoral Researcher**

Introduction

The impacts of climate change on the frequency and severity of physical hazards are putting many communities at risk. As the threat of climate change grows, so too does the need for accessible information, tools, and expertise to support climate-resilient decision making across multiple scales, from communities to countries. Woodwell Climate Research Center believes there is a need to localize and customize climate risk assessments. This information is critical for local government leaders as they make planning decisions, but it is not available to all communities. Woodwell believes that this science should be freely and widely available. To address this gap, Woodwell works with communities and countries across the world, including Ethiopia, to provide community climate risk assessments, free of charge.



Ethiopia, with its rich cultural heritage and about 126.5 million people (2023¹), faces growing climate challenges that also impact its economic priorities and natural resources. Located on the horn of Africa, Ethiopia boasts a diverse range of climates, from tropical forest in the southwest to desert in the north. Rain-fed agriculture forms the livelihoods of many of Ethiopia's communities—agriculture accounted for nearly 35% of Ethiopia's GDP in 2020.² Ethiopia experiences the effects of increased climate variability through extreme hazards including droughts, floods, and landslides across different parts of the country.

Ethiopia has established a strong policy landscape for climate action through several strategic initiatives. The national government has demonstrated their commitment to addressing Ethiopia's climate future by embracing the Sendai Framework for Disaster Risk Reduction and incorporating resilience principles into its first Nationally Determined Contribution (NDC) to the UNFCCC submitted in 2017 and revised in 2022. In addition, Ethiopia has outlined its commitment to sustainable development through key policy frameworks, including the Ten-Year Development Plan (2021–2030), the Long-Term Low Carbon Emission Development Strategy (LT-LEDS 2020–2050), the Climate Resilient Green Economy Strategy (CRGE), and the National Adaptation Plan (NAP), aimed at mitigating risks associated with climate change and environmental degradation. Woodwell's quantitative risk assessment of extreme precipitation, flooding, drought, and streamflow patterns builds upon Ethiopia's deep knowledge systems and aims to complement existing national frameworks. This report intends to provide local data insights to support decision-makers and communities to take evidence-informed approaches for resilience.

¹ World Bank, 2024

² FAO, 2024

The climate of Ethiopia is heavily influenced by its imposing topography. The country can be roughly divided into the highlands that make up most of the western half of Ethiopia and the lowlands which consist of southeast and northeast Ethiopia. These two zones differ significantly in the distribution, intensity, and seasonality of rainfall. This variation affects water availability, agriculture, and climate resilience across the country. The highlands generally see around 1,500 mm of rainfall per year (Figure 1) which falls mostly during the Kirempt season (June–September). The lowlands receive considerably less rainfall, about 300 mm annually, which occurs largely during the Belg rainy season (February–May).

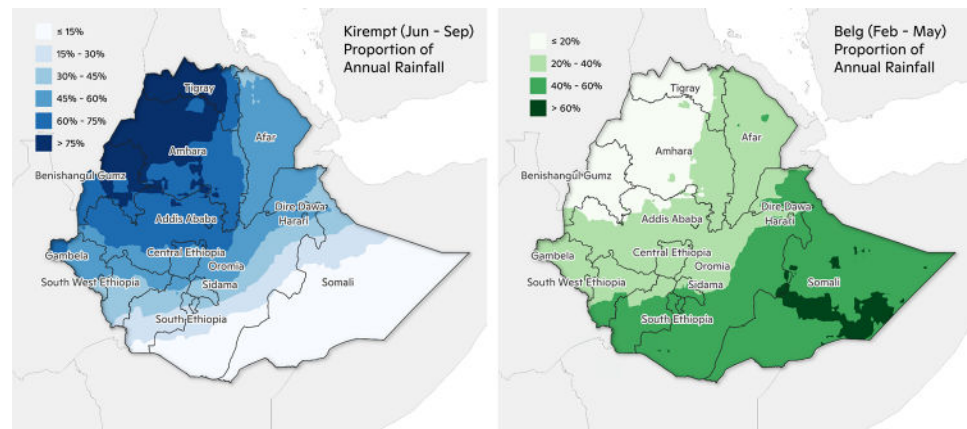


Figure 1 The spatial distribution of rainfall for the Kirempt (Jun–Sep) and Belg (Feb–May) rainfall seasons as a proportion of annual rainfall using MSWEP data (see Methodology for details on data source).

Due to this sharp gradient in annual rainfall, the type of agriculture to support livelihoods differs between the highlands and the lowlands. Crop-based agriculture dominates the highlands (Figure 2), while as one moves southeast and northeast towards the lowlands, pastoral communities become more prevalent. Approximately 94% of Ethiopia’s crop production occurs in the Meher season (September–February) which is largely a product of the Kirempt rainy season.³ A failure of the summer rains would be devastating for the Ethiopian people, especially since more than 85% of the labor force is engaged in the agricultural sector, with only 5% of crop production is irrigated, making the sector highly dependent on rainfall.⁴ Internal climate variability can lead to large swings in annual rainfall from year to year leading to a drought prone environment. Additionally, bursts of extreme precipitation that cause flooding can occur in drought years resulting in concurrent disaster events.

³ CSA, 2016a; CSA, 2016b

⁴ Chandrasekharan et al., 2021

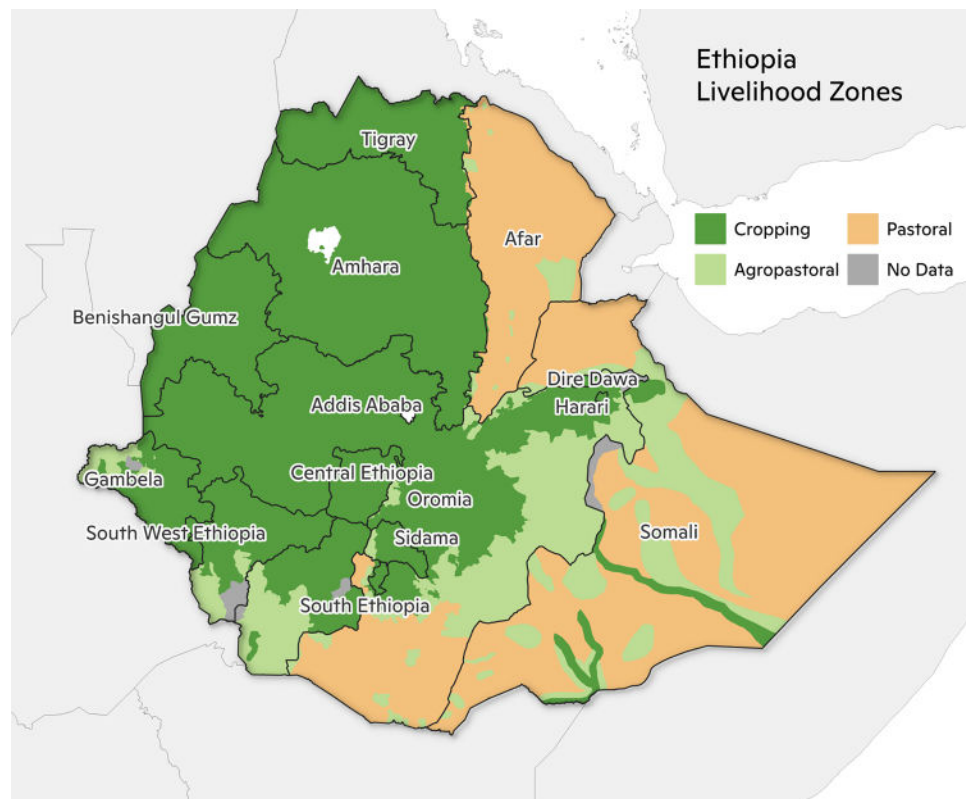


Figure 2 Source: Government of Ethiopia, USAID.

Results summary

We assess impacts across three time periods in this analysis: a historical period (labeled 2000), a near future time period (labeled 2050) and a late future time period (labeled 2070). These correspond to warming levels of 1.1°C, 2.6°C, and 3.6°C, respectively, relative to the preindustrial period (1850-1900). Future results are based on the fossil-fuel intensive SSP5-8.5 scenario; see Methodology for further information.

We show that climate change will reshape weather patterns across Ethiopia, posing significant challenges to water availability, agriculture, and livelihoods. The projected increased frequency and intensity of extreme weather events, particularly droughts and floods, will impact both highland and lowland communities. Extreme drought risk will increase moderately (1x-1.5x historical probability) in Somali by 2050 and significantly (1.5x-2x historical probability) in northwestern Ethiopia by 2070. Mean annual streamflow, low flows, and high flows in the north central portion of the country are projected to increase in volume. Extreme precipitation will also intensify with the historical 100-year rainfall amount increasing 20%-30% by 2050 and 30%-40% by 2070 for the majority of Ethiopia. Flood risk is generally concentrated within the central Rift Valley of the country and in Somali where communities have developed within the floodplain. We estimate that the 100-year flood will impact more than 840,000 structures and cause greater than \$1.2 billion 2020 USD (\$1.47 billion in 2025 USD), or more than 47 billion 2020 Birr (192 billion in 2025 Birr)⁵, in building damages.

⁵ Exchange rate was accessed on March 11, 2025. The 2020 exchange rate was taken from [Wise](#).

With the inclusion of additional local data, the climate change projections and risk metrics within this report can be generated at high resolutions for additional parts of the country, and with greater accuracy, to provide even more actionable information for policymakers. Here we present our findings on drought, streamflow, extreme precipitation, and flooding to help Ethiopia in its plans to create a more resilient future for all residents.

Drought

Between 2001 and 2021, improvements in crop yields have allowed cereal production in Ethiopia to outpace population growth. This has led to stable food security for most of the population in the highlands where cropping agriculture is prevalent (Figure 3). Between July 2009 and September 2024, much of the Ethiopian highlands spent less than 10% of the time (<18 months) in a food insecurity crisis.⁶ The lowlands, on the other hand, have experienced significantly more food insecurity. The northern half of Afar, eastern Oromia, and most of Somali have seen crisis-level, or worse, food insecurity 50%-60% (8 years-9.5 years) or more of the time between July 2009 and September 2024. Eastern portions of Amhara as well as South Ethiopia have also experienced crisis-level food insecurity between 20% (~3 years) and 40% (~6.5 years) of the 18 years analyzed. At the same time, recurrent food insecurity cannot be attributed solely to drought conditions, as multiple factors often interact. Economic, social, and political factors also play critical roles. Nevertheless, the significant impact of drought remains undeniable. For example, the 2020-2022 conflict in northern Ethiopia demonstrates how instability further exacerbates food insecurity. While a meteorological drought is a moment in time, the communities affected by drought continue to feel the impacts as infrastructure, markets, and social systems work to rebuild.

Pastoral areas are heavily reliant on livestock for income and daily food intake. Milk is a crucial form of calories and protein with young children receiving two-thirds of needed energy and all required protein from milk in Somali.⁷ In Afar, milk is the main source of protein, and livestock is often used as a trade commodity in exchange for cereals.⁸ Yet, milk production in Ethiopia, at 276 liters per cow, lags behind global annual yields (the worldwide average is 2,500 liters per cow⁹). In Somali, milk production lags even more, with a cow producing 156 liters of milk per year.¹⁰ The 2015 drought that heavily impacted northeastern Ethiopia illustrated just how much food security is tied to the success of expected rains.¹¹ In Tigray, cow milk production fell 27% in 2015 compared to the previous year. Similarly, Somali saw a 26% reduction in cow milk production over the same period.¹² The size of cattle herds in Afar decreased by 20% between 2014 and 2016, and cattle numbers did not recover to pre-drought levels until 2018.¹³ However, the Ethiopian government plans to quadruple milk production from 2022 levels by 2031 through improved feeds, strengthening milk safety and transport systems, and enhancing herd health and husbandry practices.¹⁴

The 2015 drought also brought diminished crop yields across northeastern Ethiopia. Between the 2014 and 2015 Meher seasons, grain crop production fell 66% in Afar, 10% in Tigray, and 25% in Somali.¹⁵ Eastern portions of Oromia and Amhara also faced crop losses, although not as pronounced as those in the more arid parts of the country. While there remains a significant gap between current and potential cereal yields, the Ethiopian government is actively and aggressively working to bridge that divide on several fronts such as the CRGE Strategy. As an example, current national average maize yields stand at 4.6 tons per hectare while potential yield has been estimated to be 15 tons per hectare.¹⁶ Crop yields are expected to continue to outpace population growth as has occurred for

⁶ Crisis (Phase 3) is defined as “high or above-usual acute malnutrition” or “marginally able to meet minimum food needs but only by depleting essential livelihood assets or through crisis-coping strategies.” IPC.

⁷ Sadler and Catley, 2009

⁸ Hirata et al., 2017

⁹ AHDB, 2018

¹⁰ CSA, 2017

¹¹ The 2021-2023 drought, considered worse than the 2015 drought, was not evaluated here because agricultural surveys for 2022 and 2023 have not been released by the Ethiopian Central Statistical Agency.

¹² CSA, 2014; CSA, 2015

¹³ CSA, 2016; CSA, 2018

¹⁴ Ethiopian Ministry of Agriculture, 2023

¹⁵ CSA, 2014; CSA, 2015

¹⁶ CSA, 2022; Global Yield Gap Atlas

the past two decades (Figure 4). However, even with this historical trend, it would be incorrect to assume that food security is guaranteed, as other factors must be considered such as food distribution challenges, post-harvest losses, market access constraints, and regional disparities in production.

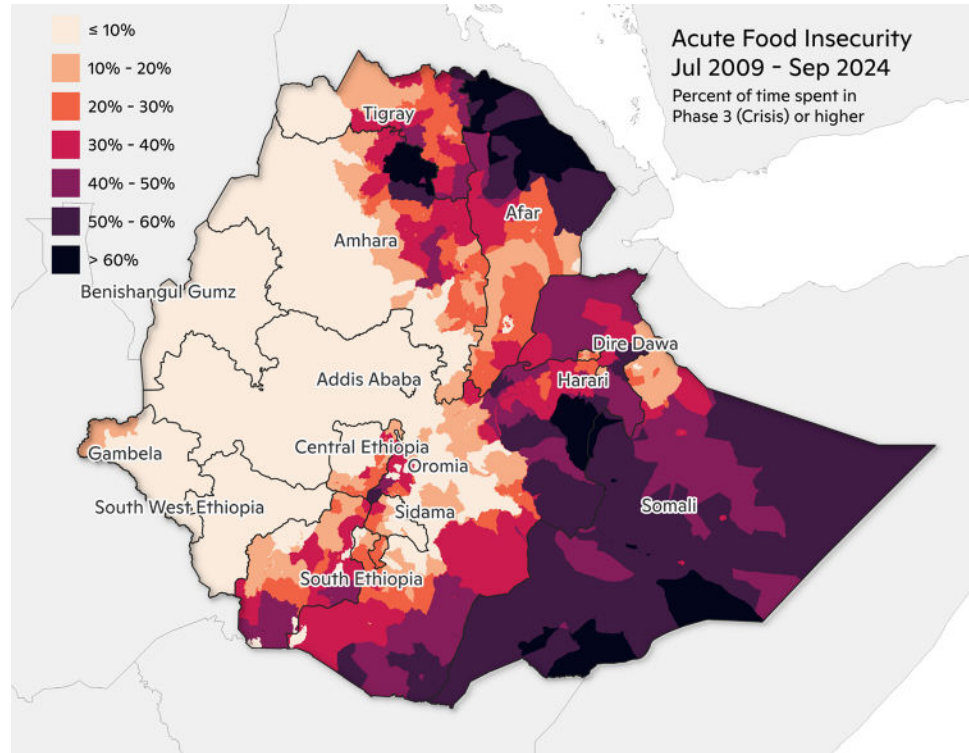


Figure 3 Source: FEWSNet, Nov 2020–Nov 2022 data is excluded. As of this writing, data from FEWSNet is not available, so any update beyond September 2024 is not possible.

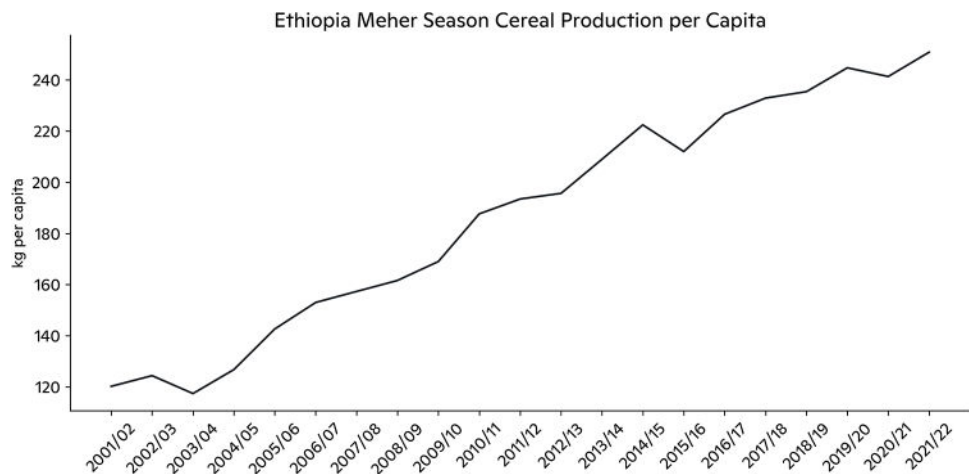


Figure 4 Graph of Meher season total production (tons) per capita for five main cereals (teff, barley, wheat, maize, and sorghum) in Ethiopia (2001–2021). Source: Population data from UN Data Portal and grain production data from Bezabih et al., 2023.

In our analysis of future drought risk, we define an extreme drought for a location (a gridcell of ~25 km) as the 10th percentile of the Standardized Precipitation-Evapotranspiration Index (SPEI) of the previous 12 months for the 1991-2010 time period.¹⁷ This would be equivalent to an annual drought with a 10-year return period. Compared to the year 2000, the vast majority of pastoral lands in Ethiopia will be subject to increased risk of extreme drought by 2050 (Figure 5). Some lowland areas will see the probability of extreme drought increase by 50% while much of the highlands are projected to experience 25% to 50% reductions in extreme drought probability. By 2070, drought risk outcomes will become inverted compared to 2050. Northwest Ethiopia, comprising Tigray, Amhara, and Benishangul Gumz, will see the probability of extreme drought increase between 50% and 100% compared to the year 2000. That is, the 10-year drought will become a 5-year drought for some communities including those surrounding Lake Bakili in Afar and the Mareb River in Tigray (e.g., the communities of Golonco and Kidus Mikael) as well as northeast of Lake Tana in Amhara (e.g., the communities of Guhala and Dudubba). While it can be useful to compare return periods of historical droughts (i.e., 2015 and 2021-2023) with projected changes in drought probability, we refrain from doing so here because of the spatial and temporal differences in drought events and the metrics used to measure those events. These disparities could lead to confusing and conflicting results as attribution studies have used different drought metrics and previous droughts have occurred in different parts of the country for different lengths of time. For example, the 2015 drought mostly impacted the northeastern quadrant of Ethiopia and was attributed a return period between 60 and several hundred years using daily precipitation rates.¹⁸ Conversely, Somali bore the brunt of the 2021-2023 drought and was estimated to be a 26-year event using SPEI, but was described as the worst drought in 40 years.¹⁹

¹⁷The 10th percentile of SPEI is used to determine dry periods because of its prevalent use as a measure of an extreme event (Wen et al., 2024). SPEI takes into account potential evapotranspiration which represents the amount of moisture that the surface could lose due to heat and radiation, and precipitation to estimate the water balance (see the Methodology section for a detailed description).

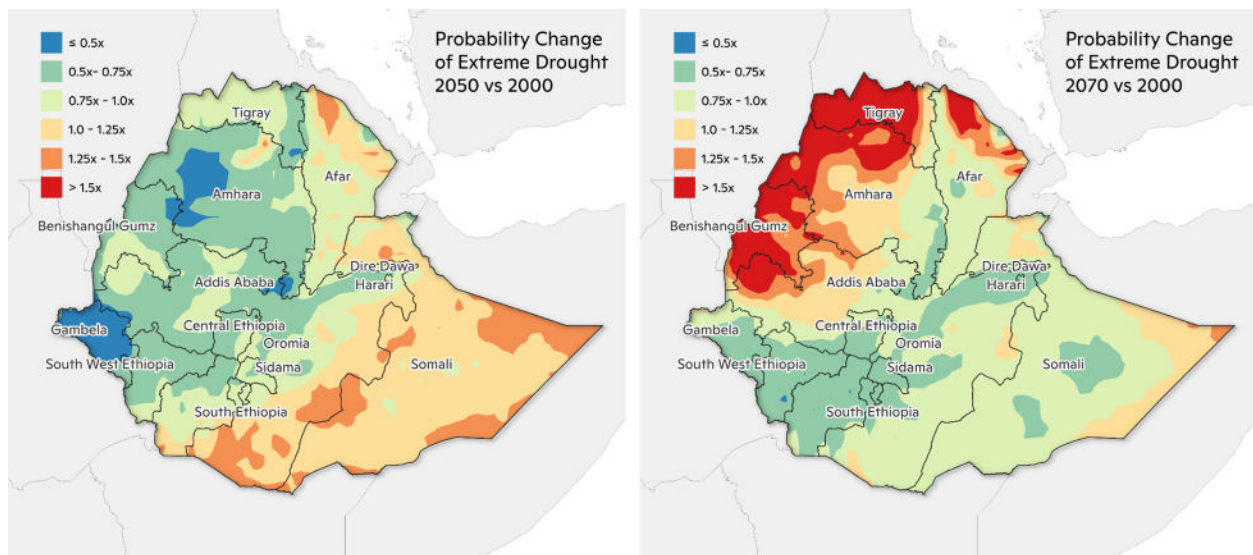


Figure 5 Change in the probability of historical extreme drought between 2000 and 2050 (left) and 2000 and 2070 (right) under SSP5-8.5. Green and blue areas represent decreasing probability while yellow and red areas indicate increasing probability.

¹⁸Philip et al., 2018

¹⁹Kimutai et al., 2025; UN News, 2022

²⁰Burek et al., 2020

Future drought probability patterns are in part attributable to changes in evapotranspiration (ET). ET is the flux of water from the earth's surface (including land, water, and vegetation) to the atmosphere and is one of the primary terms subtracted in a

water budget calculation. Annual total ET, averaged across years, was simulated using the hydrologic model CWatM²⁰ for a subregion of north central Ethiopia (hereafter referred to as the modeling domain). Further details regarding the model and methods are available in the Streamflow and Methodology sections. During the current period (1981–2019; 2000), annual ET has been moderate (0.4 to 0.8 m/yr) in the southern portion of Tigray, northern and eastern Amhara, and eastern Oromia (Figure 6). Annual ET in western Oromia and eastern Benishangul Gumz has been high (0.8 to 1.4 m/yr) relative to global annual ET values.

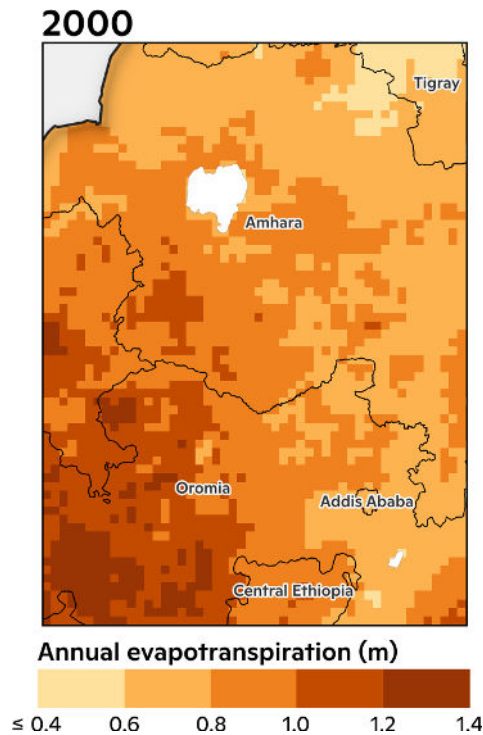


Figure 6 Current 2000 period (1981–2019) mean of annual total evapotranspiration as simulated by CWatM.

Relative to the current period, changes in annual ET in 2050 are characterized by a mix of moderate increases and decreases across the modeling domain (Figure 7). The lack of substantial change in ET, combined with projected increases in annual precipitation (Figure 8) contribute to the decrease in drought risk across the modeling domain in 2050. In contrast, almost the entire modeling domain is projected to experience increases in annual ET by 2070, with the largest increases (15% or more) projected for the eastern edge. Substantial increases in annual ET contribute to the increase in drought probability across the modeling domain under the later time period.

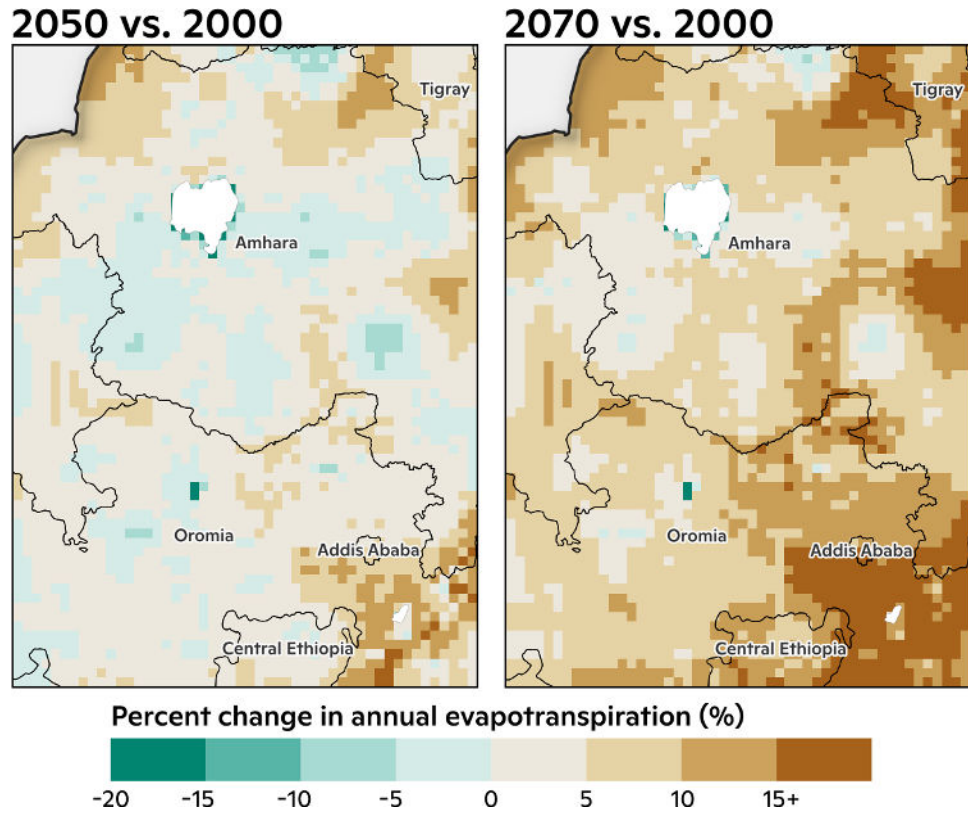


Figure 7 Percent change in period-averaged annual total evapotranspiration as simulated by CWatM between 2000 (1981–2019) and 2050 (2041–2060) (left) and 2000 and 2070 (2061–2080) (right).

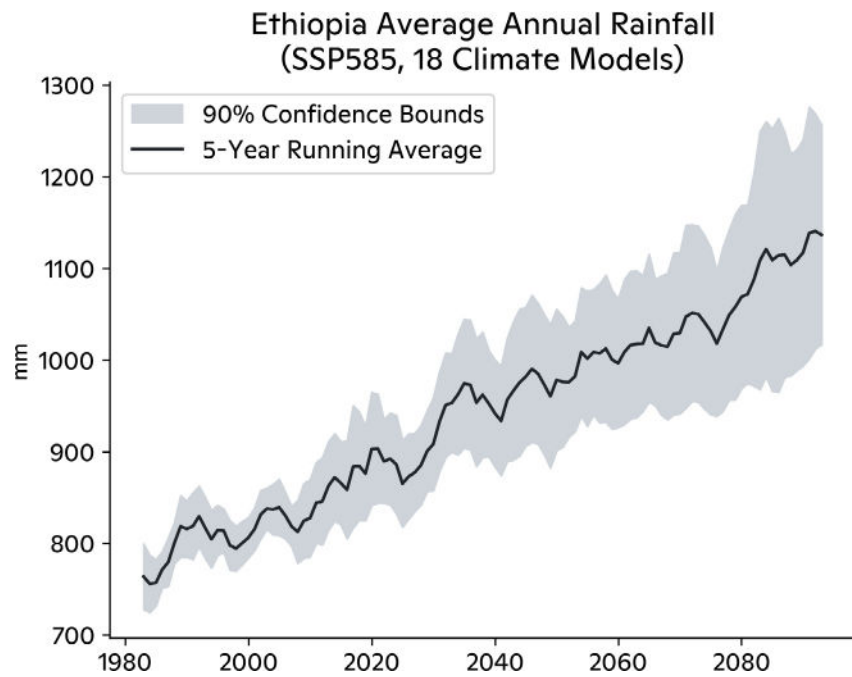


Figure 8 Spatially averaged annual rainfall for Ethiopia through 2090 under SSP5-8.5 using data from UK CEDA (see Methodology for details). The 5-year running average is shown as the bold black line and the 90% confidence bounds across the 18 CMIP6 models are shown as the gray band.

Streamflow

To assess future changes in regional hydrology, we used the large-scale hydrological model CWatM.²¹ CWatM was developed at the International Institute for Applied Systems Analysis (IIASA) in Austria and has been widely used to address questions of changing drought risk, groundwater levels, streamflow, water stress, and water supply. Streamflow was modeled for two basins: the Blue Nile River upstream of the gauge at Mendaya and the Tekeze River upstream of the gauge at Tekeze (Figure 9). These basins were purposefully chosen because they had high quality streamflow observations with which to calibrate the model, and the model performed well in both calibration and validation in these basins (see Methodology). CWatM was run for three time periods: 1981-2019 (2000), 2041-2060 (2050), and 2061-2080 (2070). The future runs are composed of twenty separate model runs, each forced by outputs from a different general circulation model (GCM) under the SSP5-8.5 scenario.

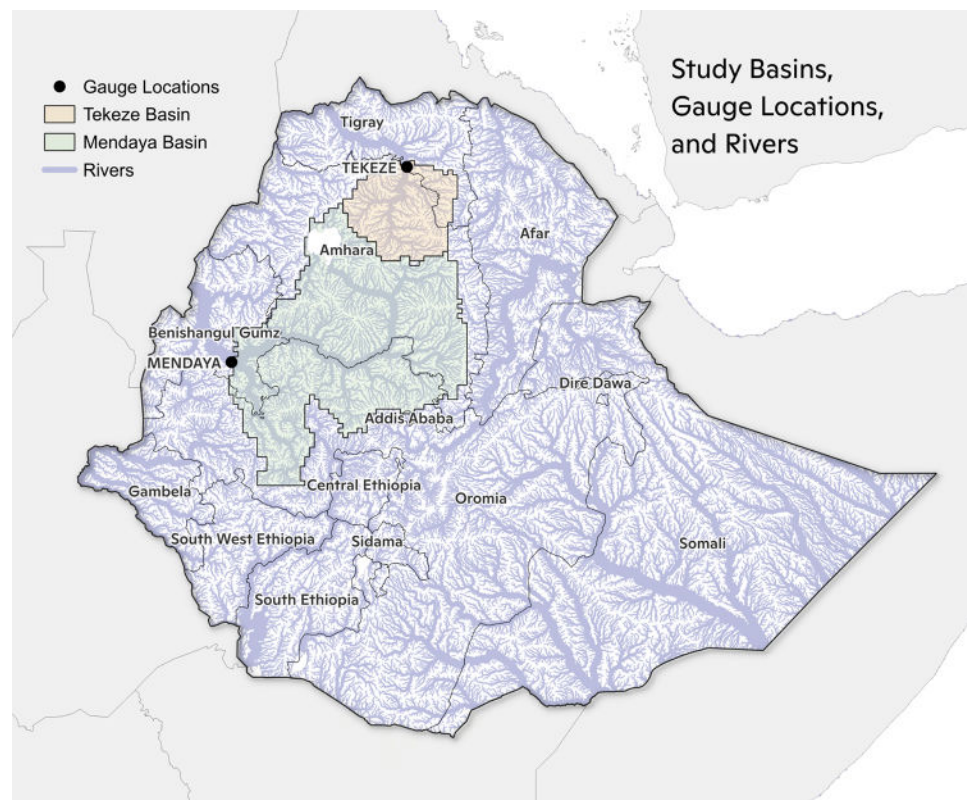


Figure 9 Map of basins used in hydrological modeling. The watershed of the Blue Nile River above Mendaya is shown in light green and the watershed of the Tekeze River above Tekeze is shown in light orange. Large black points mark the gauge locations where discharge observations were available for each basin.

Currently, flow at Mendaya and Tekeze is characterized by low flow volumes November through June and a high flow season July through October (Figure 10). The seasonality of flows is expected to persist largely unchanged under mid- and late-century projections. However, the magnitude of flows is projected to change substantially (Figures 10 and 11). Annual mean flows at the two gauges are projected to roughly double, and annual 7-day mean minimum flows are projected to increase by 60-100%. Annual 7-day mean maximum flows are projected to be 2x as large at Mendaya and more than 2.5x as large

²¹Burek et al., 2020

at Tekeze. There is a considerable range of projections across the GCMs, and although some future years may have lower high flows than some current period years, all GCMs projected higher time period-averaged high flows than what has been seen in the current period. For both locations the differences in flow metrics between the 2050 and 2070 time periods were small.

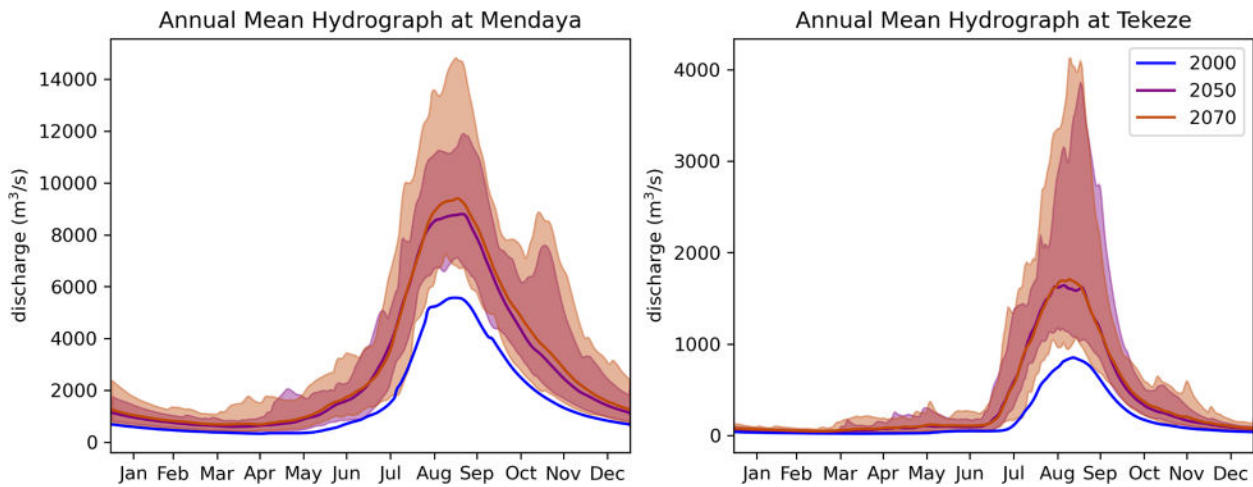


Figure 10 Annual mean hydrographs for the Blue Nile River at Mendaya (left) and the Tekeze River at Tekeze (right). The blue line shows the average across years in the current period (1981–2019). The purple and brown lines show the average across 20 GCMs and all years in the 2050 (2041–2060) and 2070 (2061–2080) periods, respectively. Purple and brown shading indicates the full range of individual GCM annual mean hydrographs for the 2050 and 2070 periods, respectively.

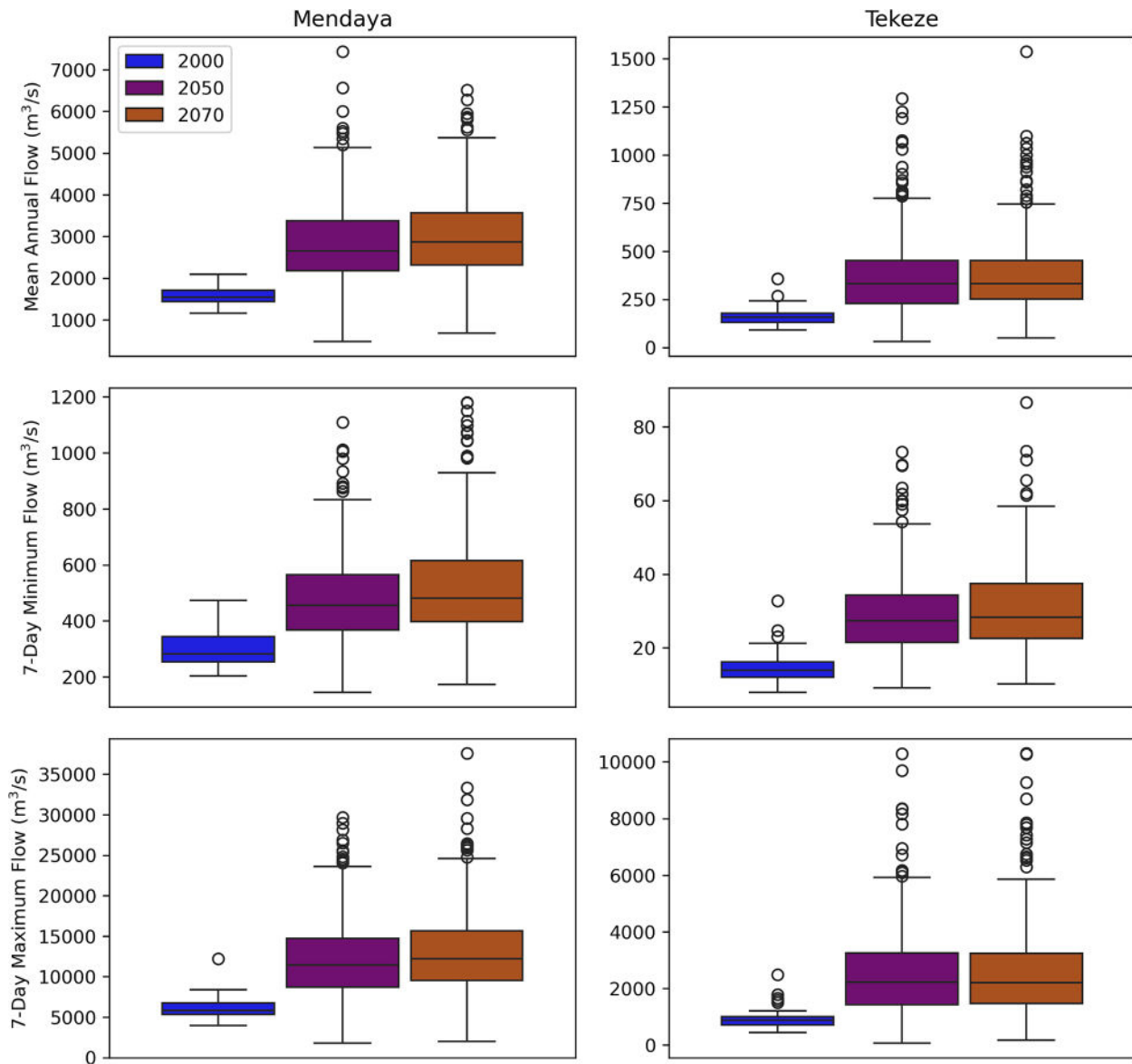


Figure 11 Distributions of mean, minimum and maximum streamflow metrics (rows) under three time periods for the Blue Nile River at Mendaya (left column) and the Tekeze River at Tekeze (right column). Boxplots represent the distribution of yearly values in each period, or the distribution of yearly values across all GCMs in the case of future time periods. Whiskers extend a distance of 1.5 times the interquartile range from the box, which covers the interquartile range.

Trends in flow metrics at the two gauges were indicative of projected changes across northwest Ethiopia (Figures 12-17, Table 1). Averaged across the modeled domain, mean annual flow was projected to increase by 20 m^3/s (129%) by 2050 and 23 m^3/s (144%) by 2070 (Table 1). The magnitude of projected increases was roughly proportional to the current flow volume such that larger rivers were projected to see larger increases in mean annual flow (Figures 12, 13). Relative changes in mean annual flow were projected to be largest in the northeastern and southeastern corners of the modeling domain (not shown).

Absolute Changes (m³/s)			
	Mean Flow	Minimum Flow	Maximum Flow
2050 vs 2000	+20	+3	+58
2070 vs 2000	+23	+4	+68
Relative Changes (%)			
	Mean Flow	Minimum Flow*	Maximum Flow
2050 vs 2000	+129	+942700	+71
2070 vs 2000	+144	+1822000	+80

Table 1 Modeling domain-averaged changes in flow metrics. *Relative changes in minimum flows should be viewed with caution since they entail division by near-zero current period values in some locations. For reference, a 100% increase in flow means the future flow is 2x the current flow volume.

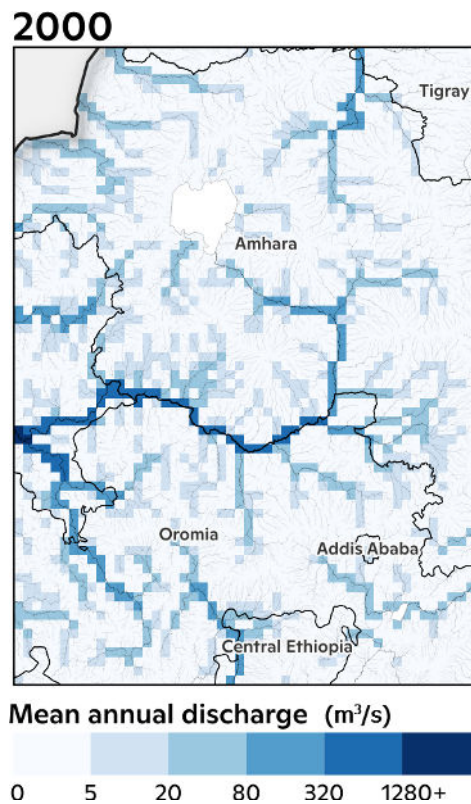


Figure 12 Mean annual discharge during the current 2000 period (1981–2019). Discharge data is visualized on the CWatM grid. Faint lines show the river network.

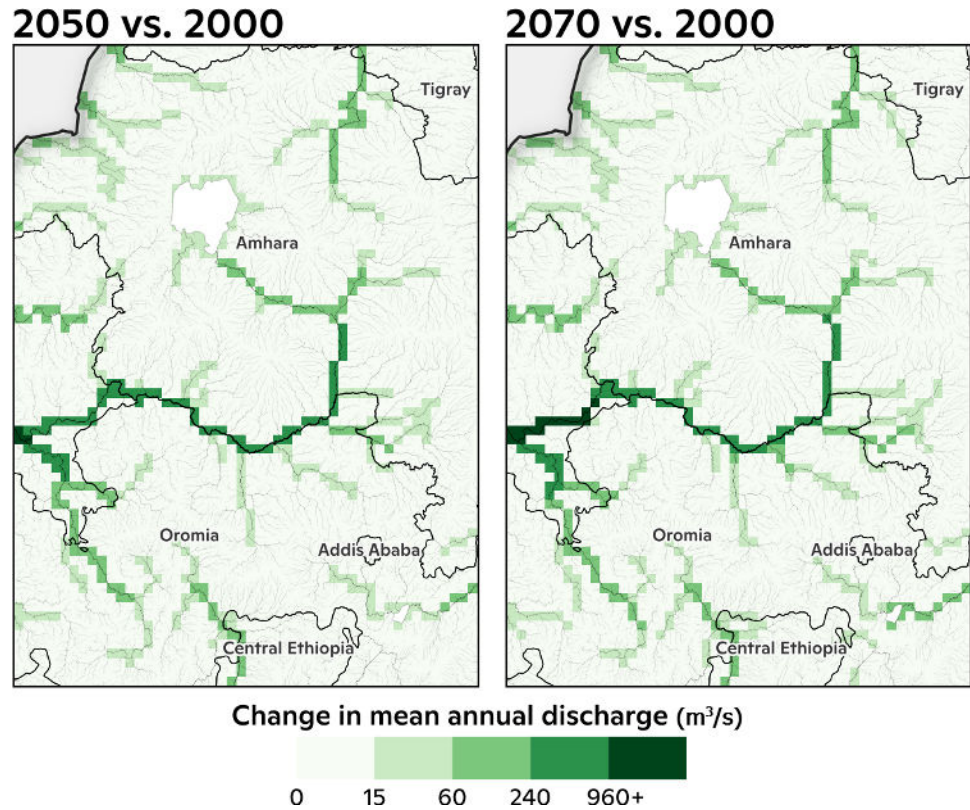
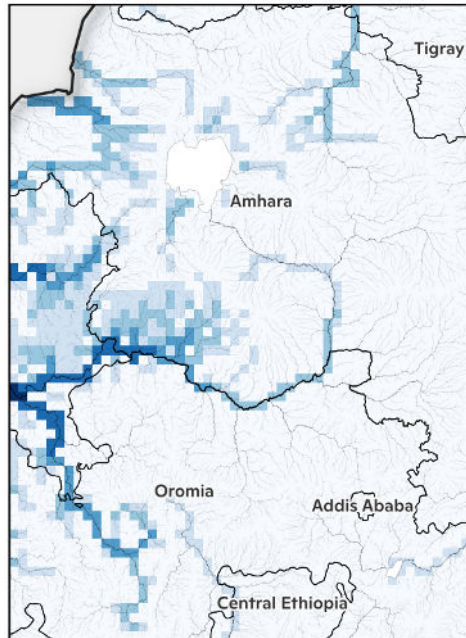


Figure 13 Change in mean annual discharge during the 2050 period (2041–2060) compared to the current 2000 period (1981–2019) (left) and the 2070 period (2061–2080) compared to the current period (right). Discharge data is visualized on the CWatM grid. Faint lines show the river network.

Currently, the annual 7-day mean minimum flows (hereafter low flows) are highest on the main river branches and in the western portion of the modeling domain (Figure 14). Looking at the projected changes in low flows, there was little difference between the 2050 and 2070 projections; low flows were projected to increase by 3 m³/s and 4 m³/s by 2050 and 2070, respectively, with the largest increases on the main river branches (Table 1, Figure 15).

2000



Minimum annual discharge (m³/s)

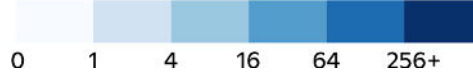
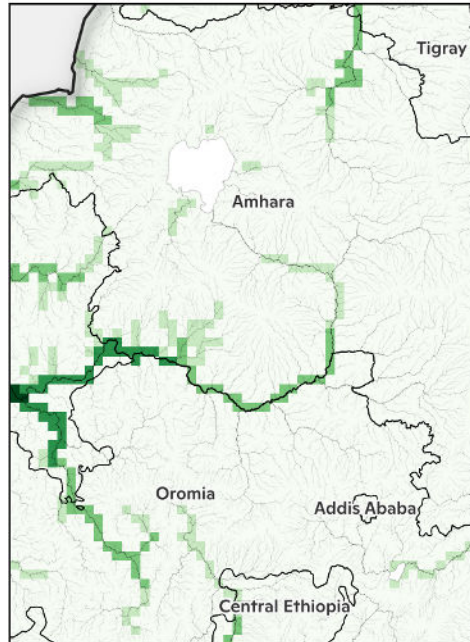
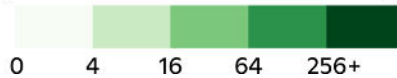


Figure 14 Mean annual 7-day minimum discharge during the current period (1981–2019). Discharge data is visualized on the CWatM grid. Faint lines show the river network.

2050 vs. 2000



Change in minimum annual discharge (m³/s)



2070 vs. 2000

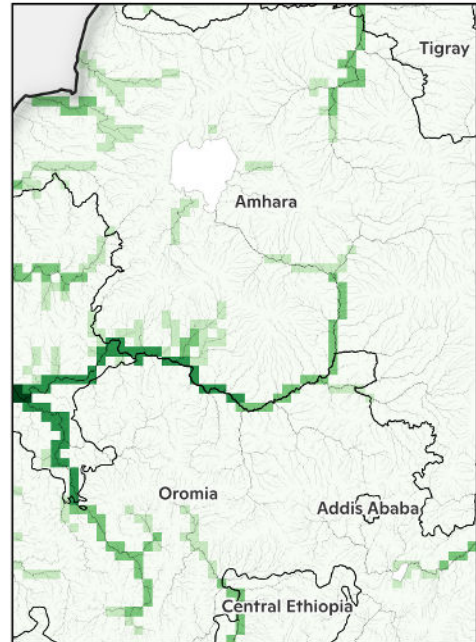


Figure 15 Change in mean annual 7-day minimum discharge during the 2050 period (2041–2060) compared to the current period (1981–2019) (left) and the 2070 period (2061–2080) compared to the current period (right). Discharge data is visualized on the CWatM grid. Faint lines show the river network.

The annual 7-day mean maximum flows (hereafter high flows) are currently highest on the Blue Nile River, with values $> 5000 \text{ m}^3/\text{s}$ near Mendiya (Figure 16). Averaged across the modeling domain, high flows were projected to increase by $58 \text{ m}^3/\text{s}$ (71%) and $68 \text{ m}^3/\text{s}$ (80%) by 2050 and 2070, respectively (Table 1). The greatest absolute high flow increases ($> 2500 \text{ m}^3/\text{s}$) were projected for the Blue Nile River (Figure 17), while the greatest relative increases (100-200% or more) were projected for the northern third of the study domain (not shown).

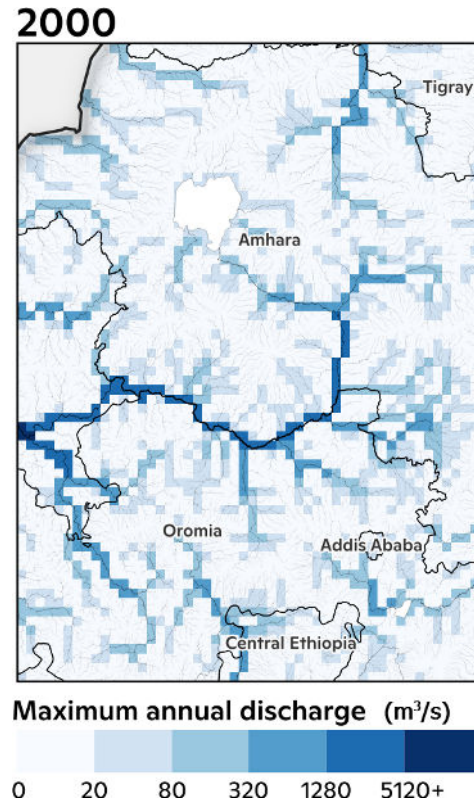


Figure 16 Mean annual 7-day maximum discharge during the current period (1981–2019). Discharge data is visualized on the CWatM grid. Faint lines show the river network.

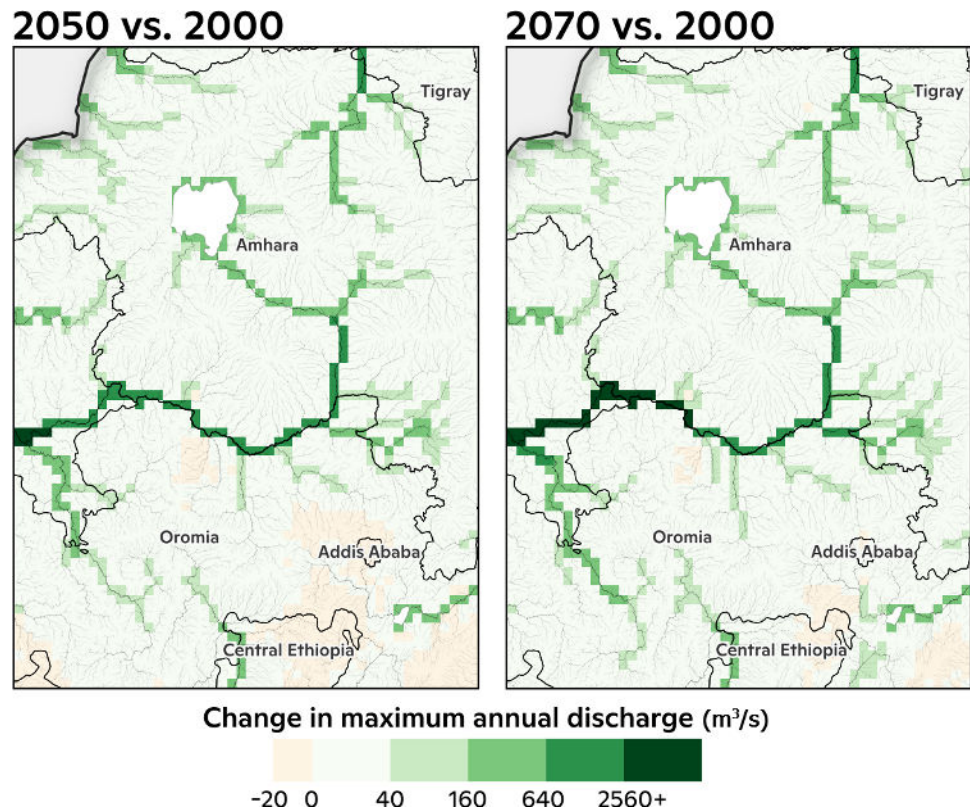


Figure 17 Change in mean annual 7-day maximum discharge during the 2050 period (2041–2060) compared to the current period (1981–2019) (left) and the 2070 period (2061–2080) compared to the current period (right). Discharge data is visualized on the CWatM grid. Faint lines show the river network.

Increased mean flow volumes will increase hydropower generation potential across the modeling domain. However, infrastructure such as dams and turbines may need to be adapted in order to take advantage of greater water availability. Greater flow volumes may also help to reduce potential for water conflicts related to competing uses, such as hydropower and irrigation. Modest increases in low flow volumes may enhance the seasonal consistency of water availability, benefiting biodiversity as well human water uses. Large increases in high flow volumes may present a risk to lives, livelihoods, and infrastructure, and these risks should be investigated further. Additionally, increased flows will likely mobilize higher sediment loads which has implications for reservoir storage capacity unless sediment release is incorporated into dam infrastructure planning.

Extreme rainfall

Current extreme rainfall estimates are derived from the Multi-Source Weighted-Ensemble Precipitation (MSWEP) dataset. The 100-year 1-day rainfall event is used as the metric to represent extreme precipitation because it is commonly used in the scientific community and the regulatory frameworks of many countries. From the MSWEP dataset (Figure 18) we see that the greatest rainfall amounts for the 100-year event occur in central Ethiopia around Addis Ababa, southern Amhara, and central Oromia. High rainfall amounts are also present in Gambela, South Ethiopia, and central Somali. The 100-year rainfall amounts generally trace the path of the Simien Mountains in northern Ethiopia and the Amhar Mountains in central Ethiopia. However, the lack of smoother gradients between areas of high rainfall amounts and low rainfall amounts is likely due to spatial artifacts

caused by limited incorporation of rainfall gauges in MSWEP for Ethiopia. Therefore, this result is likely an incomplete picture of extreme rainfall risk.

The present-day 100-year 1-day rainfall amount is expected to increase between 20% and 30% by 2050 for much of Ethiopia including eastern Oromia, South Ethiopia, most of Amhara, Dire Dawa, and Harari while 30% to 40% increases are projected in eastern Tigray (Figure 19). Additionally, the probability of the current 100-year event is expected to at least double by 2050 (Figure 20). In those same areas, the 100-year event will become a 50-year, 40-year, and even a 30-year event. By 2070, the present day 100-year rainfall amount will be at least 30% greater for the majority of the country with the highest increases in northeast Ethiopia. Eastern Tigray, for example, is projected to see rainfall amounts increase by more than 50%. Similar intensification is expected for the probability of the current 100-year rainfall event for 2070. Most of Ethiopia is projected to see the present day 100-year rainfall event become at least a 40-year event while Amhara, Dire Dawa, Tigray, Afar, and eastern Oromia will see even greater intensification with return periods reaching 20-year in some areas.

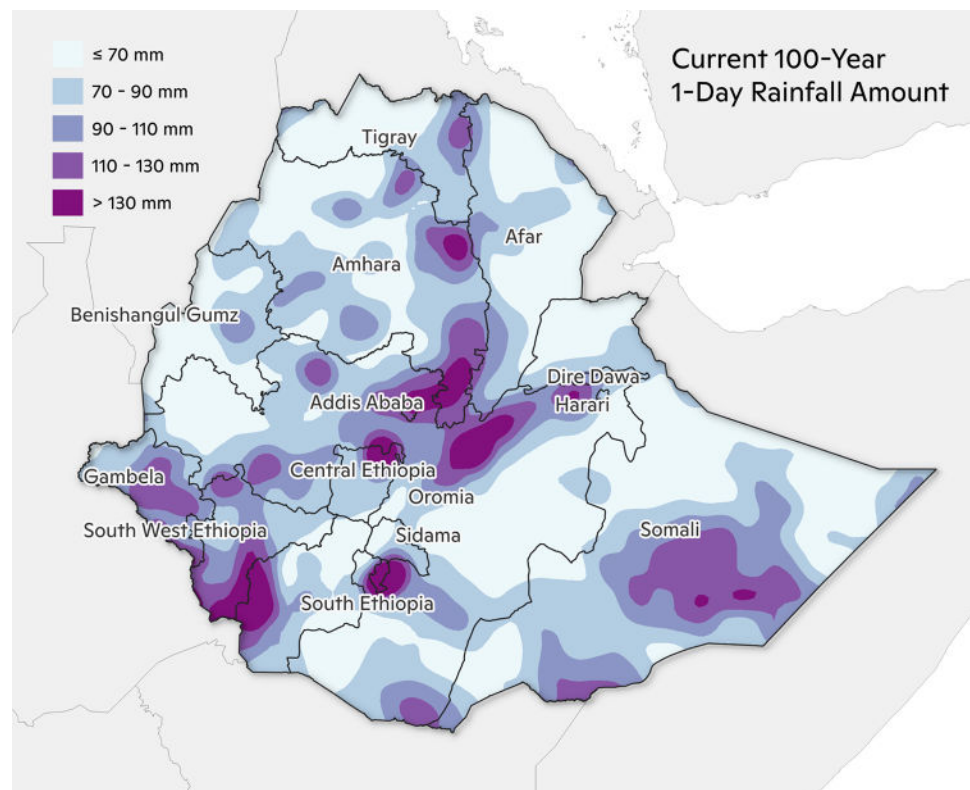


Figure 18 The 100-year 1-day rainfall amount in mm based on daily MSWEP data from 1979–2020.

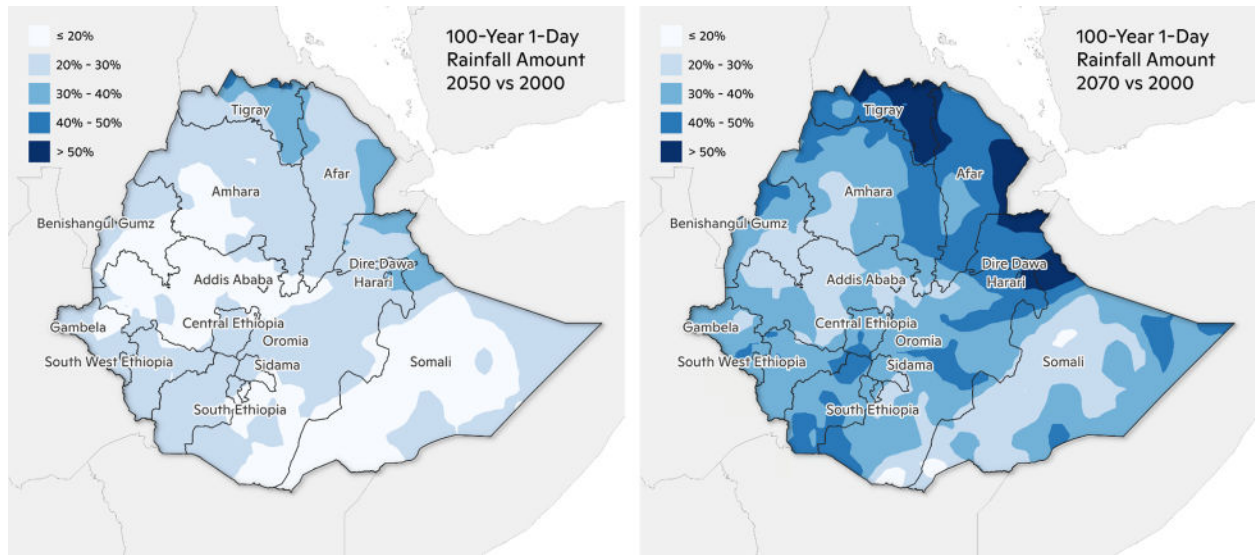


Figure 19 Percent increase of the 100-year 1-day rainfall event between 2000 and 2050 (left) and 2070 (right) under SSP5-8.5.

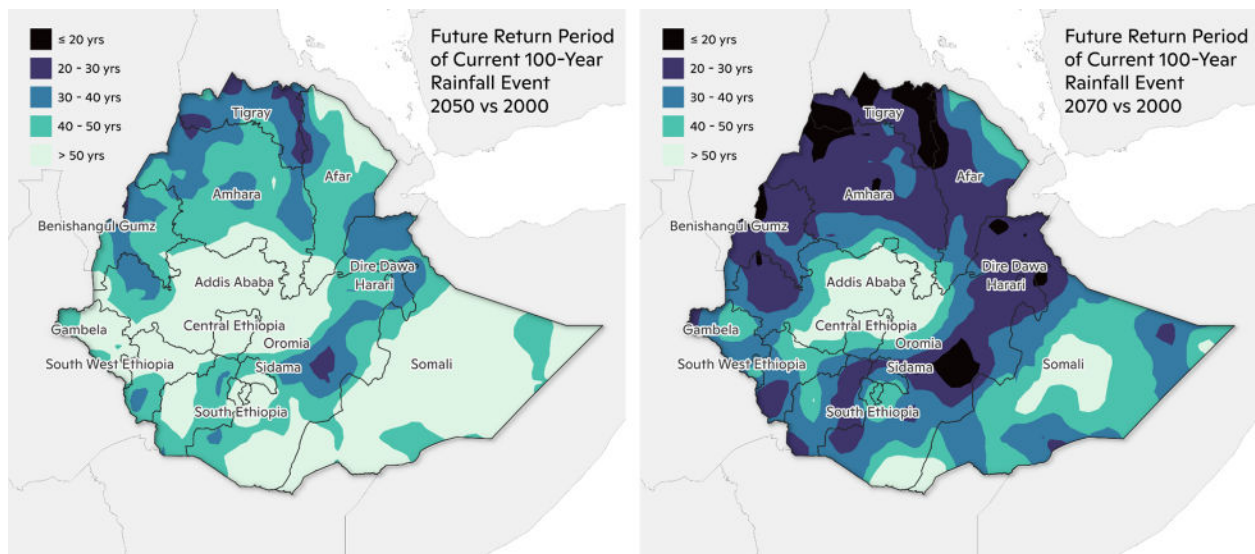


Figure 20 Future return period of the current (2000) 100-year 1-day rainfall event for 2050 (left) and 2070 (right) under SSP5-8.5.

Flood

While Ethiopia’s rivers provide an abundant resource for hydroelectric generation, they are also a source of severe flood risk. Many buildings and farms have been developed within floodplains leaving communities at risk of flood events. Over 5.6 million people have been affected by floods in Ethiopia since 2000 with flood events occurring in 19 out of the last 25 years.²² While building values are concentrated in urban areas (Figure 21) such as Addis Ababa, Bahir Dar, Dire Dawa, and Jijiga, the greatest flood losses can often be in rural areas. The Rift Valley within Oromia, South Ethiopia, Central Ethiopia, Tigray, and Amhara is one of these high risk areas as well as the Awash River basin, the Shebelle River basin, Dire Dawa, and the Farar river floodplain (Figure 22). Overall, the

²²EM-DAT

100-year flood in Ethiopia impacts more than 840,000 structures and causes greater than \$1.2 billion 2020 USD (\$1.47 billion in 2025 USD) in building damages. Riverine flood risk (pluvial risk was omitted) was estimated using a hydrodynamic model, LISFLOOD-FP, in conjunction with depth-damage functions and a building disaggregated exposure dataset.²⁵ While agricultural and building content losses are not modeled here, incorporating flooded farmland would undoubtedly increase total damages significantly, as growing crops within floodplains is common practice (Figure 23).

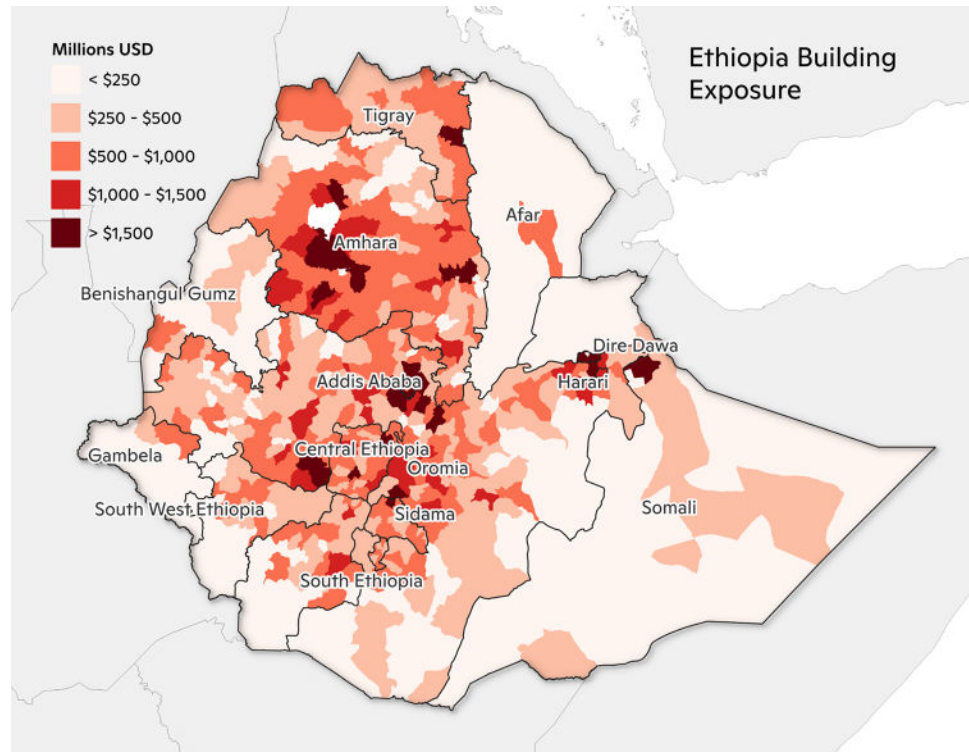


Figure 21 Building value at the zone administrative level in millions of USD 2020.

²²Damages were calculated by associating damage percentages to water depth levels for each building in Ethiopia. An exposure dataset representing building values for the year 2020 was then used to assign a construction value to each building. Damage percentages were combined with building values to estimate total building damage for the 100-year event in Ethiopia and then adjusted for inflation to 2025 USD (see Methodology section for a detailed description).

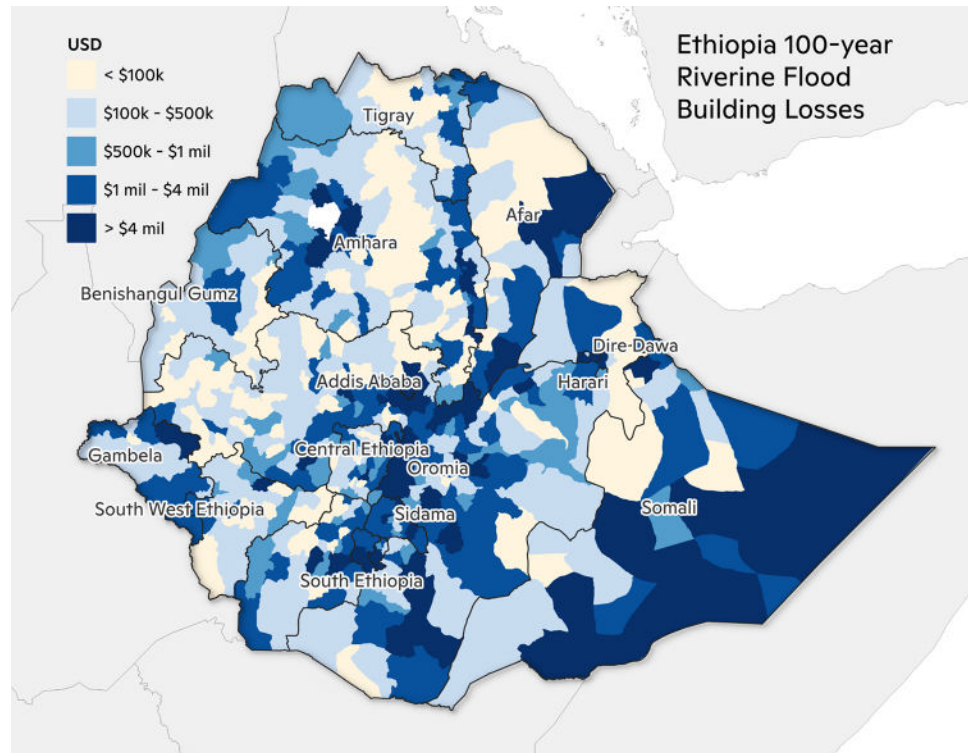


Figure 22 Building value losses from the 100-year riverine flood aggregated at the woreda level. All values are in 2020 USD. Source: Woodwell Climate Research Center.

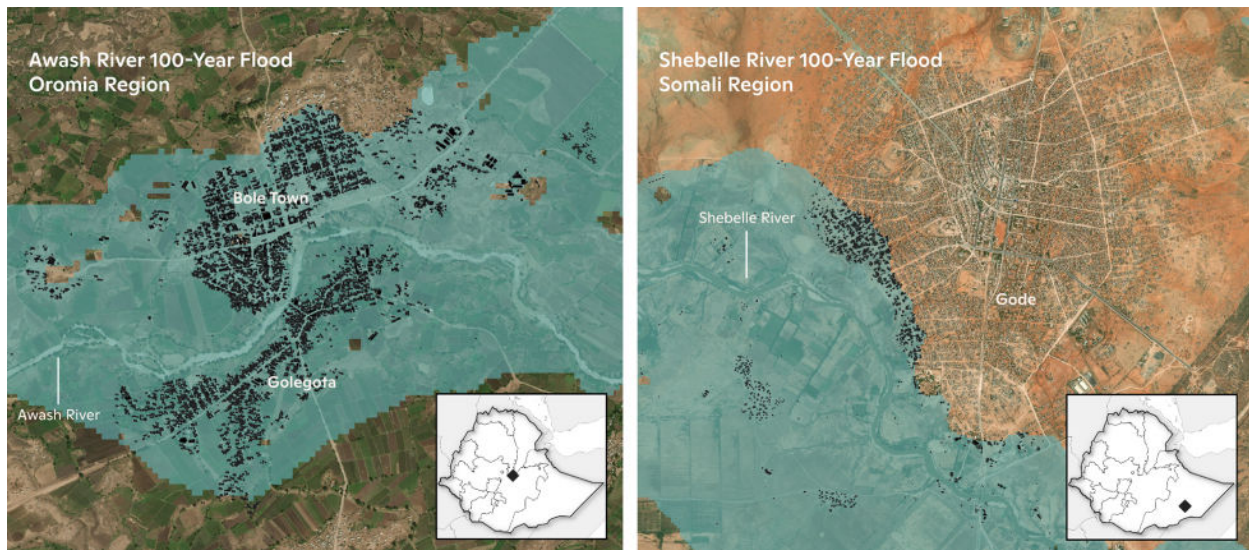


Figure 23 Inundated buildings (black points) in the Awash River, Oromia 100-year floodplain (left) and the Shebelle River, Somali 100-year floodplain (right).

Conclusion, caveats, and future work

This report explores some of the primary climate risks facing Ethiopia over the next several decades, including drought, changes in streamflow, extreme precipitation, and flooding. We find spatially heterogeneous changes in the risk of extreme drought, which

can greatly reduce yields of key nutrient sources (cereals and cow milk). Drought risk is projected to increase moderately in southeastern Ethiopia by 2050 and increase significantly in northwestern Ethiopia by 2070, despite robust increases in annual precipitation. This can be in part explained by the increased evaporative demand of a warmer atmosphere and is corroborated by the projections for evapotranspiration, which show (for the north central modeling domain) little change in evapotranspiration by 2050 but spatially averaged increases of 9% by 2070. In contrast to these drying trends, increased precipitation is projected to greatly increase the intensity and frequency of extreme precipitation events, particularly in Tigray, and to more than double mean annual streamflow volumes in north central Ethiopia. Flood risk is generally concentrated within the central Rift Valley of the country and in Somali where communities have developed within the floodplain. We estimate that the 100-year flood impacts more than 840,000 structures and causes greater than \$1.2 billion 2020 USD (\$1.47 billion in 2025 USD) in building damages.

While the combination of more dry extremes and more wet extremes may at first seem counterintuitive, this is a common storyline in climate change. A warmer atmosphere intensifies the water cycle with major impacts on two key processes: increased evaporative demand can more effectively draw remaining moisture from already dry areas enhancing drought risk, and greater atmospheric water holding capacity enables more extreme precipitation events. The new, more extreme, hydrological regime can present challenges to water management,²⁴ agricultural productivity,²⁵ and natural ecosystems.²⁶

While the analysis presented here is robust and provides a detailed view of climate risk within Ethiopia, further improvements could be made through the incorporation of additional local data. One significant adjustment would be to bias-adjust and downscale the CMIP6 models using 4 km resolution gridded data products based on station temperature and precipitation data.²⁷ Better representation of temperature and precipitation would improve projections of extreme precipitation and drought.

Such local climatological data would also assist in expanding the hydrological simulations to the entirety of Ethiopia. The hydrology modeling presented here is based on calibration of CWatM at two locations with long-term monthly streamflow observations. Compared to daily observations, monthly observations provide limited information with which to characterize streamflow discharge, contributing additional uncertainty to the calibration. The model calibration for the current modeling domain could likely be improved if there were long-term daily streamflow observations available to calibrate to. Given longer record lengths and long-term (ideally daily) streamflow observations in other parts of the country, it may be possible to extend the modeling domain to cover the entire country. Further improvements could include providing CWatM with reservoir release observations to better constrain reservoir operations and updating the reservoir layer in CWatM to include the effect of reservoirs built after 2008.

Agriculture losses from drought in this report have been presented as regional patterns with anecdotal references to historical crop and livestock losses to illustrate projected impacts. However, much more granular projections for various crops at the household level are possible by developing a crop yield model that takes into account agronomic data (e.g., yield, fertilizer application, improved seeds, irrigation), soil data from the Ethiopian Soil Information System (*EthioSIS*), terrain and high resolution climate data. This analysis would only be possible with the household data collected by the Ethiopian Central Statistical Agency for the annual Agricultural Sample Survey. This analysis could then be expanded to livestock as well to generate a complete picture of climate impacts on agriculture across Ethiopia.

²⁴Ficklin et al., 2022

²⁵Furtak and Wolińska, 2023

²⁶Sabater et al., 2022;
Knapp et al., 2008

²⁷Ethiopian Meteorological
Institute

Flood risk studies are often limited to single watersheds or cities due to the computational requirements of simulating floods at large spatial scales. As part of this analysis, we have developed a country-wide riverine flood model that provides policymakers with much wider scope and higher resolution (30 meters) than previously available. Still, there are several pathways for improving the flood risk assessment that were not incorporated in this report due to data unavailability. First, incorporating local digital elevation models (DEMs) from LiDAR and the recently released FathomDEM²⁸ where LiDAR is not available would increase the flood model's accuracy. Second, hydro-enforcement of the DEM to represent river channels in the elevation data would simulate flows more realistically. Third, using streamflow data from gauges and a country-wide calibrated hydrology model is an important enhancement for properly estimating flooded areas. Fourth, flood risk is currently slightly underestimated due to the limited buffering extent of the simulated watersheds. This could be adjusted by increasing buffer radius for areas with large floodplains. And fifth, simulating pluvial flooding would provide a more holistic view of flood risk rather than solely focusing on riverine risk.

Developing such a flood model would allow for the creation of a catastrophe flood model. A proof-of-concept of a catastrophe model was presented in this report that estimated the damages to buildings from the 100-year flood. Simulating more flood events would be a straightforward procedure and lead to the construction of annual average loss estimates in the current and future climates. Average annual losses, and catastrophe models in general, are highly useful for policy planning, insurance procurement, and loss and damage projections. Further improvements to the catastrophe model would involve high resolution building exposure data (i.e., commercial vs industrial areas), localized depth-damage functions, and high resolution agriculture exposure data (i.e., crop production at the household level).

The focus of this report has been future climate projections to inform long-term policymaking. However, there is also room for analysis that would benefit operational and day-to-day disaster prevention. For instance, Google's DeepMind recently released GenCast, a probabilistic weather model that uses machine learning to generate forecasts.²⁹ Such models have been shown to outperform state-of-the-art numerical models in less computational time. Incorporating such a tool into disaster prevention and response operations would bring greater flexibility and reduce resources required for weather forecasting. Another operational focused analysis would be the creation of indices specifically for parametric insurance against drought and flooding. A large number of Ethiopian households participate in parametric insurance programs.³⁰ With the uptake of insurance products likely increasing in the future, climate indices that accurately represent a loss in income are important to reduce basis risk in parametric products.³¹ Creation of new metrics, such as flooded areas using satellite imagery, will also be crucial for expanding parametric insurance access.

This report provides actionable data insights that enable decision-makers and communities to plan for resilience strategies, though some of the model's effectiveness and accuracy could be further improved with the incorporation of additional local data. The report highlights the need for various policies and measures, but building drought- and flood-resilient systems with advanced, AI-integrated prediction tools stands out as a top priority. This risk assessment establishes patterns in extreme precipitation, flooding, drought, and streamflow, enhancing Ethiopia's deep knowledge systems and providing evidence for the implementation and strengthening of existing national frameworks.

²⁸Uhe et al., 2025

²⁹Price et al., 2024

³⁰World Food Programme

³¹PwC, 2024

Methodology

Throughout this report we use the CMIP6 SSP5-8.5 scenario, a fossil-fuel intensive pathway. We consider three time periods in this analysis: a historical period (early 1980s to mid-late 2010s depending on the climate variable; labeled 2000), a near future time period (2041–2060; labeled 2050) and a late future time period (2061–2080, labeled 2070). Under the SSP5-8.5 scenario, these periods correspond to projected warming of 1.1°C, 2.6°C, and 3.6°C, respectively, relative to the preindustrial period (1850–1900). These levels serve as guideposts for climate policy. Consider the Paris Accord, the main global climate framework whose goal is to limit warming to no more than 1.5°C. Given that both 2023 and 2024 exceeded 1.5°C—and that policies-in-place are on track for closer to 3.0°C of warming with extreme outcomes closer to 4.5°C, exploring higher warming levels is warranted. This is especially useful given recent changes in climate ambition and uncertainty surrounding the timing, impact, and interaction of climate tipping points.

Extreme Precipitation

In this report, we present results for future-projected extreme rainfall using a nonstationary (NS) methodology for various intensity-duration-frequency (IDF) curves. In a NS approach, precipitation estimates are calculated for the entire time period (i.e., 1971–2100) using a temporal parameter to represent changes in extreme precipitation through time. The NS approach is well suited for engineering applications as future relative changes are more realistic compared to a quasistationary approach which compares two rainfall distributions built from two distinct time periods according to the United States National Oceanic and Atmospheric Administration (NOAA).³³

The data used in this analysis consist of daily precipitation data from 18 Coupled Model Intercomparison Project Phase 6 (CMIP6) climate models for the SSP5-8.5 warming scenario that has been bias-adjusted and downscaled to 25-km resolution over Ethiopia using a Bias Correction Constructed Analogues with Quantile mapping reordering (BCCAQ) method³⁴ and MSWEP observation data (hereafter referred to as UK CEDA). BCCAQ is a combination of two bias adjustment methods which allows for effective replication of extreme events and spatial covariance at daily time steps.³⁵ MSWEP was chosen as the historical precipitation dataset from four observational datasets and UK CEDA was chosen as the projected downscaled climate model dataset for this study from 5 downscaled climate model datasets due to their ability to most accurately represent the distribution of historical country-wide averages of annual rainfall and historical spatial patterns of average annual rainfall. In Figure 24 we show the distribution of annual rainfall from 1981 to 2014 from 10 different rainfall datasets which includes historical only datasets (Abebe (2017), ERA5, CHELSA, CHELSA-W5E5, and MSWEP) as well as downscaled climate model sources and methodologies (Carbon Plan, Climate Impact Lab, ISIMIP, NASA NEX, and UK CEDA).³⁶ We use the Abebe (2017) dataset as the groundtruth since the dataset only used rainfall gauge data. Among the historical-only data, the distributions of CHELSA-W5E5 and MSWEP most closely resemble the distribution of Abebe (2017). We chose MSWEP instead of CHELSA-W5E5 due to its documented strong performance in representing daily rainfall from radar³⁷ and rainfall gauges³⁸ which is important for extreme precipitation analyses.

Among downscaled climate model datasets, three resemble the distribution of annual rainfall of Abebe (2017): ISIMIP, NASA NEX, and UK CEDA. To select one product from these three datasets, we considered the spatial patterns of average annual rainfall over 1981–2014 across Ethiopia (Figure 25). We removed NASA NEX from consideration given

³²Zhong and Rojanasakul, 2024; Wunderling et al., 2024

³³NOAA, 2022

³⁴Gebrechorkos et al., 2023

³⁵Gebrechorkos et al., 2023

³⁶Abebe, 2017; ERA5; CHELSA; CHELSA-W5E5; GLoH20, 2024; Carbon Plan; Climate Impact Lab; Bias-adjustment and downscaling of CMIP6 models was done using ISIMIP methods from Lange (2019) and Lange (2021) with CHELSA-W5E5 observational data; NASA NEX

³⁷Beck et al., 2019

³⁸Beck et al., 2017

that it shows little spatial heterogeneity of rainfall. While ISIMIP is a higher resolution dataset, initial tests of this dataset in the extreme precipitation estimation framework revealed spatial artifacts leaving UK CEDA as the final choice for estimating future extreme precipitation in Ethiopia.

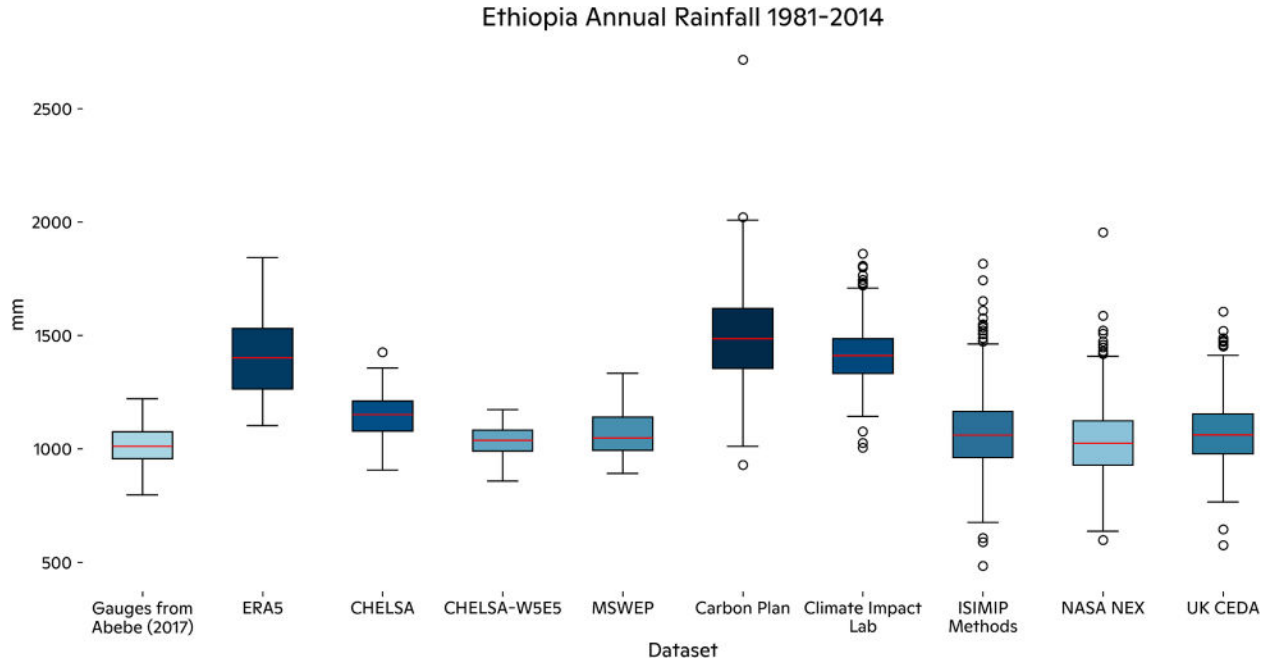


Figure 24 Ethiopia annual rainfall distribution for 1981–2014 from 10 data sources. Box plots with lighter hues represent distributions with lower means while box plots with darker hues represent distributions with higher means.

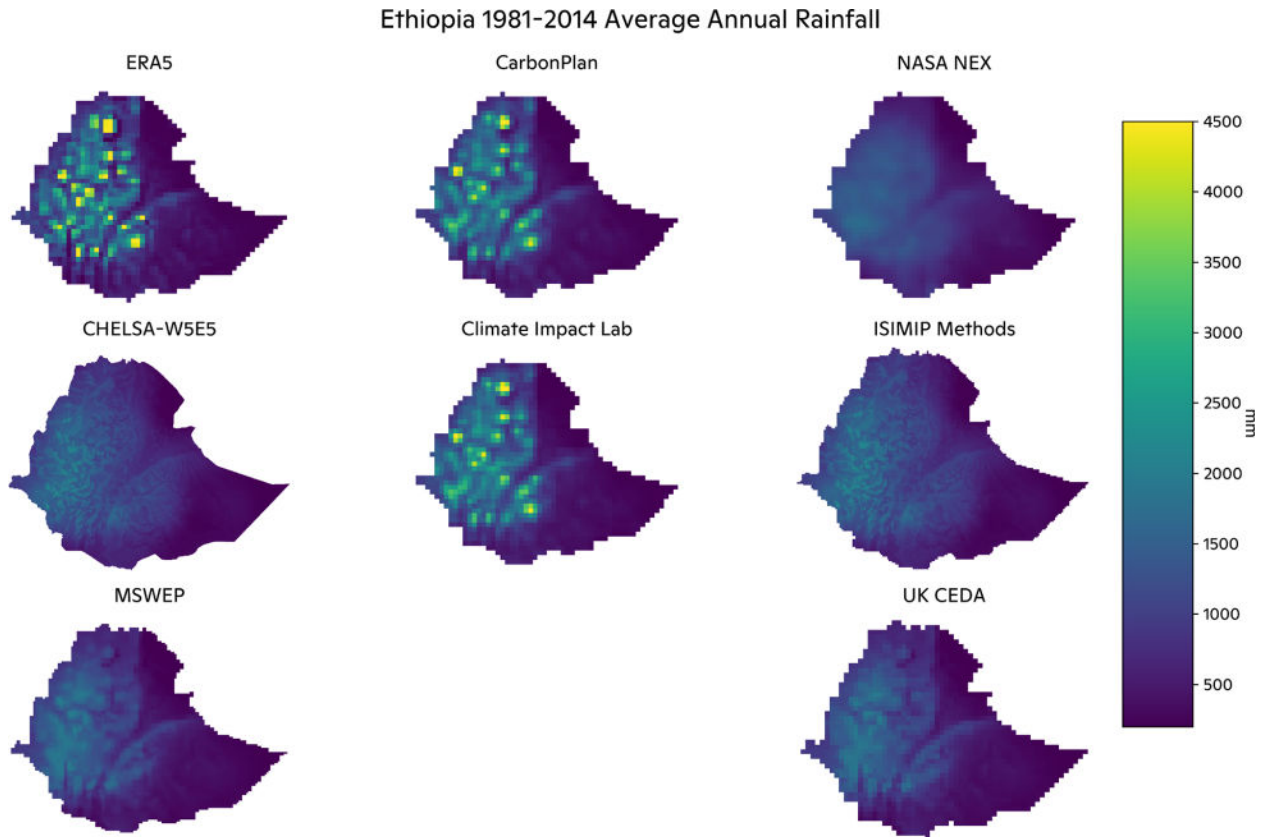


Figure 25 Ethiopia average annual rainfall from 1981–2014 from 8 different sources.

We use a perimetric fitting method to estimate the parameters of the Generalized Extreme Value (GEV) distribution. For each target pixel, a 40-mile radius is used to capture the annual maxima of the surrounding pixels. Each pixel's surrounding annual maxima is given a weight using a triweight kernel function based on distance (e.g., pixels ≥ 40 miles have zero weight). The log-likelihood function of the GEV distribution is then minimized with the Nelder-Mead algorithm using the annual maxima and pixel weights to estimate the GEV parameters. The beta distribution of penalized coefficients ranging between -0.5 and 0.5 is used to constrict the shape parameter as specified by NOAA.³⁹

To estimate future daily precipitation frequency estimates (PFEs), the biases (ratio) between the baseline period and the MSWEP daily PFEs are calculated and then multiplied by the future climate model daily PFEs. The MSWEP daily PFEs are created using a perimetric method to fit the GEV distribution as was done for the CMIP6 data but for the 1979–2020 time period and with no temporal parameter.

To incorporate temporal changes through the data series, five parameters are fitted to the annual maxima of 1971–2100. The parameters are a_0 , a_1 , b_0 , b_1 , c_0 which are used to represent the GEV parameters:

$$\begin{aligned} location &= a_0 + a_1 RCP \\ scale &= \exp(b_0 + b_1 RCP) \\ shape &= c_0 \end{aligned}$$

³⁹NOAA, 2022

where RCP represents the radiative forcing under a specific scenario for each annual maximum. Radiative forcing data was acquired from the Reduced Complexity Model

Intercomparison Project (RCMIP)⁴⁰ for SSP5-8.5. Three rounds of parameter fitting were completed to ensure convergence for all pixels. The first round is solely for generating initial estimates for a_0 , b_0 , and c_0 which is done by only using those three values to represent the location, scale, and shape parameters, respectively. The GEV distribution is fitted using the entire time series (1975-2100) with the initial parameters set as location: the mean of the annual maxima series (AMS) for the target pixel; scale: the standard deviation of the AMS for the target pixel; shape: -0.1, which represents the expected value of the beta distribution.⁴¹ The natural log of the scale is used to ensure the scale is positive. In the second round of fitting, initial parameters to the optimization scheme are set as a_0 : the previously fitted location parameter for the target pixel; a_1 : zero, which represents no trend; b_0 : the previously fitted scale parameter for the target pixel; b_1 : zero, which represents no trend; c_0 : the previously fitted shape parameter for the target pixel. For the third round of fitting, the initial parameters are set as the average parameter value within a three-pixel radius around the target pixel.

Drought

Drought risk is assessed using the Vicente-Serrano's Standardized Precipitation and Evapotranspiration Index (SPEI).⁴² We first calculated potential evapotranspiration (PET) following the Hargreaves formulation. PET represents the atmospheric evaporative demand, or the amount of moisture that the surface could lose due to heat and radiation. The difference between PET and precipitation gives us an estimate of the water balance. A 12-month running sum was then applied to the water balance time series to reduce noise and capture significant anomalies. Next, the anomalies from the historical period were standardized by calendar month, thus accounting for seasonal effects. After standardization, we were able to identify the negative water balance anomaly level with 10% or less chances of occurring in the 1985-2015 (2000) time period. The 10th percentile of SPEI is used to determine dry periods because of its prevalent use as a measure of an extreme event.⁴³ This threshold was lastly used to estimate the chances of experiencing the same negative anomaly in the future time periods of 2041-2060 (2050) and 2061-2080 (2070). Similarly to the extreme precipitation analysis, the UK CEDA dataset was used for the SPEI calculation. We use SPEI as the drought metric since it considers both precipitation and PET whereas other approaches consider only precipitation (e.g. the Standardized Precipitation Index (SPI)) or only temperature and precipitation (e.g. the Palmer Drought Severity Index (PDSI)).

Streamflow and Evapotranspiration

Historical and future streamflow and evapotranspiration were modeled using the Community Water Model (CWatM⁴⁴), a large-scale hydrological model developed at the International Institute for Applied Systems Analysis (IIASA) in Austria. CWatM accounts for surface and groundwater processes, river routing, water demand, and reservoirs built before 2009. For this work, the model was run at daily temporal resolution and 5 arcmin spatial resolution.

For calibration and the historical simulation, all climate forcings except precipitation were taken from the W5E5v2.0⁴⁵ dataset. The W5E5v2.0 forcings are at 0.5° spatial resolution and include mean air temperature, minimum air temperature, maximum air temperature, surface pressure, relative humidity, wind speed, and downwelling shortwave and longwave radiation. Initial results showed better performance when using precipitation data from MSWEP instead of W5E5v2.0. MSWEP⁴⁶ precipitation data is available at 0.1° spatial resolution and had to be aggregated to the W5E5v2.0 grid to work with the other forcings. For the future periods, climate data from 20 general circulation

⁴⁰RCMIP

⁴¹Martins and Stedinger, 2000

⁴²Vicente-Serrano et al., 2010

⁴³Wen et al., 2024

⁴⁴Burek et al., 2020

⁴⁵Lange et al., 2021

⁴⁶Beck et al., 2019

models (GCMs) from the CMIP6 experiment were bias-adjusted and downscaled to 0.5° spatial resolution using the ISIMIP3BASD v2.5 methodology.⁴⁷ CWatM was run with data from the SSP5-8.5 scenario for the periods 2039–2060 and 2059–2080 to represent conditions around 2050 and 2070, respectively. The first two years of each time period were considered spinup and not included in analysis. All climate forcings were downscaled by CWatM to 5 arcmin resolution using the high resolution WorldClim⁴⁸ dataset.

CWatM was calibrated using a multi-basin, leave-future-out cross-validation approach. Two sites were selected for calibration that had long-term continuous data with no obvious errors and minimal streamflow regulation: Mendaya on the Blue Nile River (9.943°N, 35.677°E) and Tekeze on the Tekeze River (13.348°N, 38.742°E) (Figure 9). Streamflow observations for these sites were provided by the Nile Basin Secretariat.⁴⁹ The leave-future-out cross-validation entailed categorizing the observation years as warm years and cool years based on basin-averaged annual mean air temperature from W5E5v2.0. Streamflow observations from the coolest 50% of years were used for calibration and observations from the warmest 50% of years were used for validation. This approach provides insight on the model's ability to transfer to warmer future conditions.

CWatM was calibrated using the evolutionary algorithm NSGA-II⁵⁰ from the DEAP⁵¹ framework. The Kling-Gupta Efficiency⁵² (KGE) was used as the objective function. The calibration was implemented on the two basins simultaneously and the basin-mean KGE computed on the monthly cool-year streamflow time series was used as the run KGE. 18 parameters pertaining to soil water, lakes, reservoirs, and groundwater were calibrated. The calibration was run on a virtual machine with 32 cores and used an initial population size of 640 followed by 30 generations of 32 runs. The parameter settings in the best identified runs were used in the historical and future simulations.

The best calibration site-mean KGE was 0.40 and the site-mean validation KGE was 0.45. At Mendaya, the calibration and validation KGEs were 0.25 and 0.27, respectively. The simulation overestimated both low and high flows and the timing of peak flows was shifted several weeks late relative to observations (Figure 26). Further investigation is needed to understand the cause of these biases and develop a way to minimize them. At Tekeze, the calibration and validation KGEs were 0.55 and 0.64, respectively. The simulation captured low and high flows well, although the timing of peak flow was slightly later than in the observations (Figure 27). We note that CWatM accounts for the effects of Chomen Lake (a reservoir) but does not account for the Tekeze dam and reservoir since they were not completed until 2009. This did not affect the calibration, since observations before 2000 were used, however it does mean that the simulations for Tekeze represent naturalized flow.

⁴⁷Lange, 2019; Lange 2021

⁴⁸Fick and Hijmans, 2017

⁴⁹Nile Basin Initiative, 2021

⁵⁰Deb et al., 2002

⁵¹Fortin et al., 2012

⁵²Kling et al., 2012

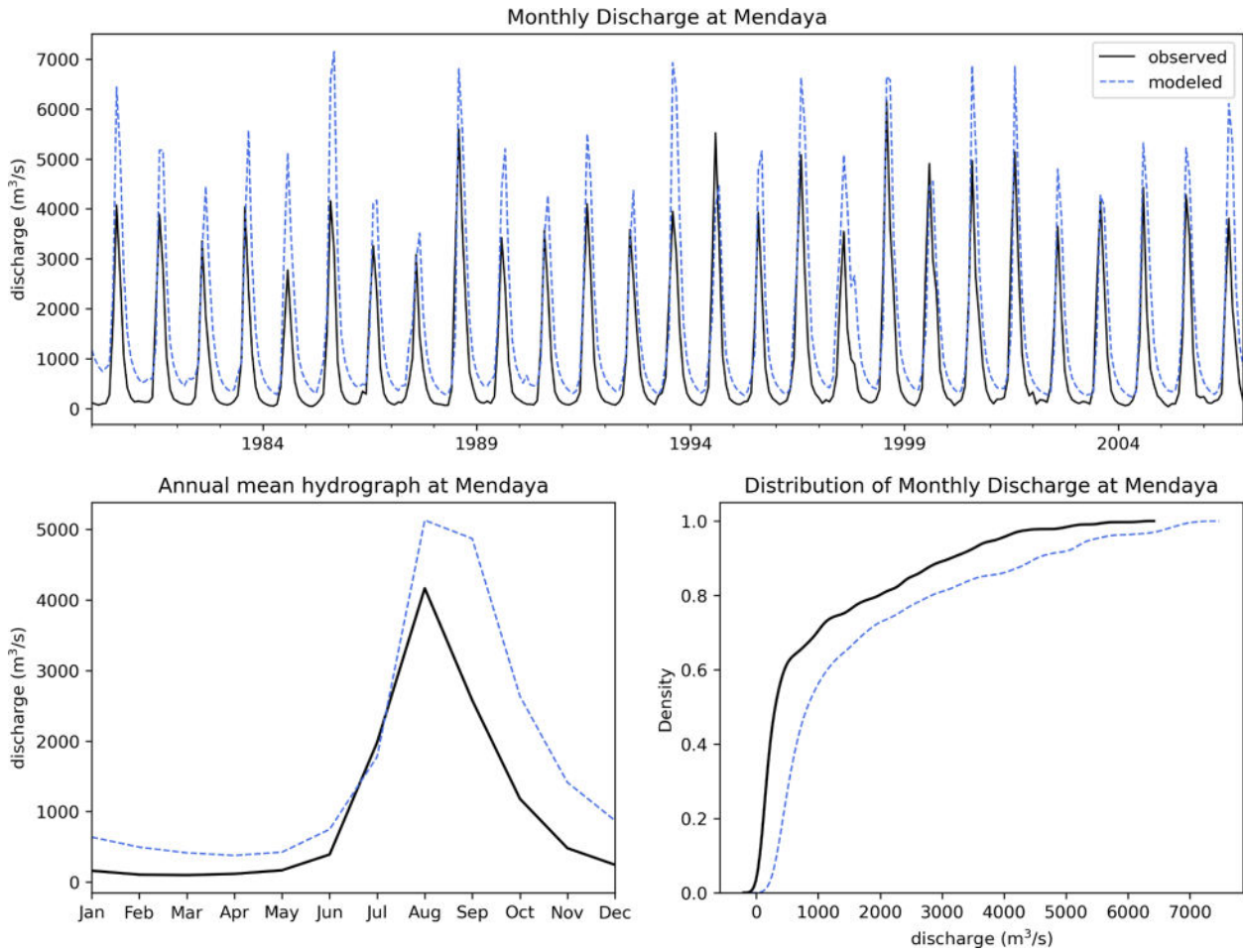


Figure 26 Comparison of monthly streamflow at Mendaya from observations (black lines) and the best simulation (blue dashed lines). The top panel shows the full time period, the bottom left panel shows the annual mean hydrograph (i.e. averaged across years), and the bottom right panel shows the cumulative density function of the two streamflow time series.

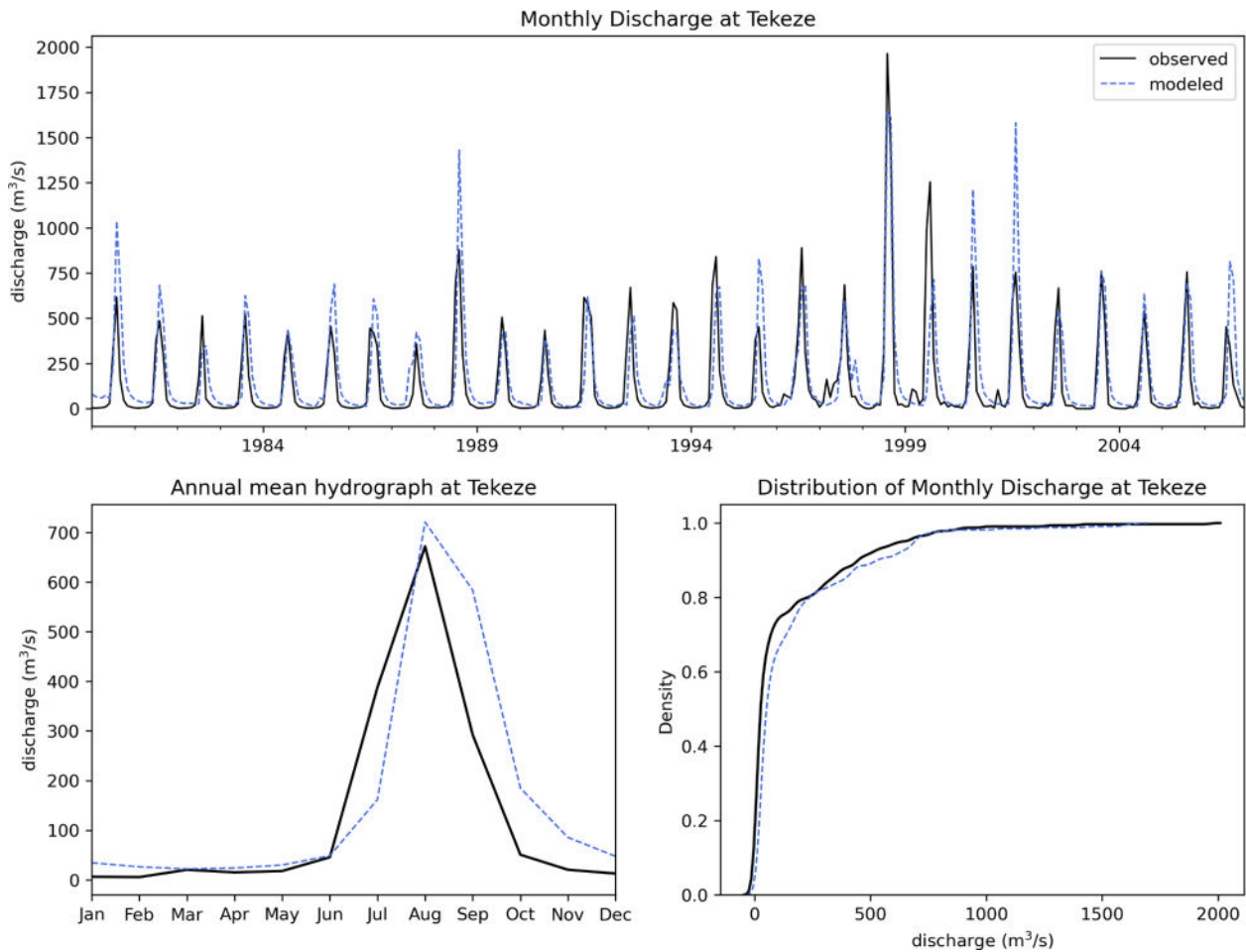


Figure 27 Comparison of monthly streamflow at Tekeze from observations (black lines) and the best simulation (blue dashed lines). The top panel shows the full time period, the bottom left panel shows the annual mean hydrograph (i.e. averaged across years), and the bottom right panel shows the cumulative density function of the two streamflow time series.

Flooding

Present day flood risk in Ethiopia is evaluated using the LISFLOOD-FP v8.1 hydrodynamic model and simulating the 100-year flood.⁵³ LISFLOOD-FP is a two-dimensional raster hydraulic model capable of solving all terms of the shallow water equations and has been extensively used from the river reach scale to continental simulations.⁵⁴ Here we use the local inertia solver of LISFLOOD-FP which neglects the convective acceleration term of the shallow water equations. The 100-year flood was chosen given its common use in the scientific literature and has been used as a regulatory floodplain standard in several countries. We solely model fluvial flood risk; however, pluvial risk could be introduced into the model at a future stage. The Forest and Buildings Removed Digital Elevation Model⁵⁵ (FABDEM) was used as the elevation data for the LISFLOOD-FP simulations. Floodplain friction values were assigned using the DynamicWorld land cover dataset from January 1, 2024. Land cover values were then converted to friction estimates using data adopted by the United States Natural Resource Conservation Service in Kansas.⁵⁶ The 100-year streamflow estimates were taken from the extreme flow data generated for different return periods by GEOGloWS v2.⁵⁷ Since flows from GEOGloWS represent 1-day averages, boundary conditions for LISFLOOD-FP were created to represent a linear

⁵³LISFLOOD-FP developers, 2022

⁵⁴Shaw et al., 2021

⁵⁵Hawker et al., 2022

⁵⁶Janssen et al., 2016

⁵⁷GEOGloWS, 2022

increase of flow for the first 8 hours of simulation time before reaching the peak flow which was maintained for the remainder of the 24-hour simulation. The flood model was not validated since historical daily streamflow was not available for reconstructing a historical event. Future analysis would include validation.

For computational efficiency, each watershed within the TDX Hydro Version 1.0 within Ethiopia, used by GEOGloWS, was modeled separately. Each watershed was given a buffer of 1 km to reduce edge effects in the final output. The model was run on a high performance cluster designed in the Google Cloud Platform environment and took approximately 48 hours to complete 59,510 watersheds. Results from all the watershed simulations were combined in the end to create a seamless raster over Ethiopia by taking the maximum value of any overlapping areas between watershed extents. To determine the financial losses from the 100-year riverine flood, an exposure dataset was created using building stock values from the SSAHARA⁵⁸ project which were then assigned to individual building footprints from the Overture Maps Foundation.⁵⁹ Exposure values represent 2020 USD. For a particular flood depth, a building loss percentage was assigned to a building using depth-damage functions for Africa developed by the European Commission Joint Research Centre.⁶⁰

Annex 1

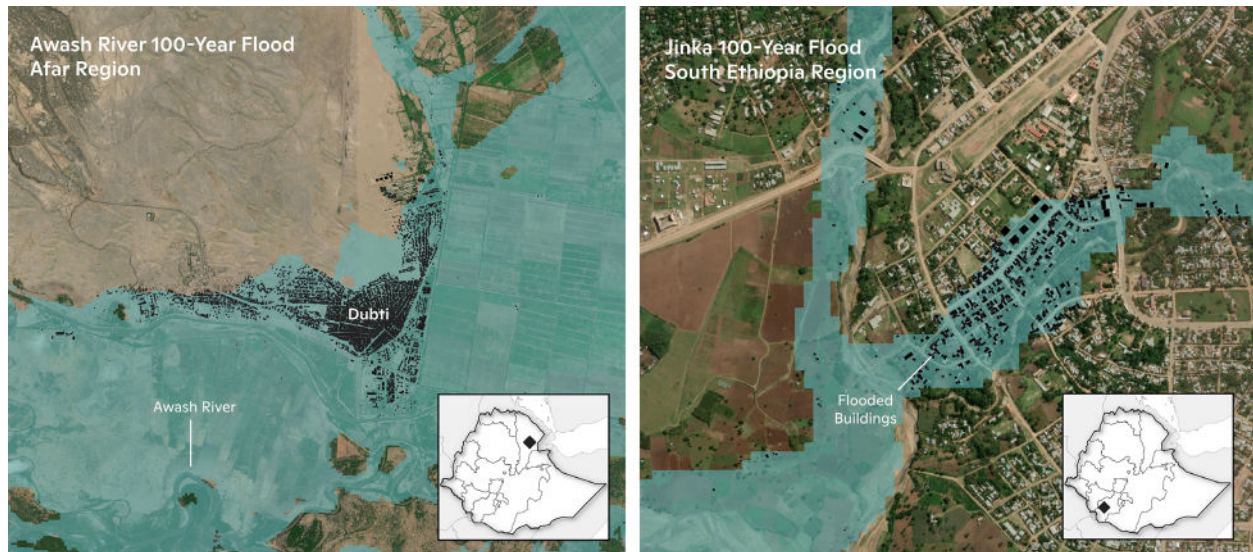


Figure A.1 Inundated buildings (black points) in the Awash River, Afar 100-year floodplain (left) and Jinka, South Ethiopia 100-year floodplain (right). Flooded buildings are denoted by black outlines.

⁵⁸SSAHARA, 2022

⁵⁹Overture Maps Foundation

⁶⁰Huizinga et al., 2017



Front cover: Residential districts with rapidly developing downtown of central business district of Ethiopian capital Addis Ababa, Ethiopia.

Back cover: Aerial view a settlement in a valley of the Lasta Mountains, Lalibela, Amhara Region, Ethiopia.

photos by Vadim Nefedov



WOODWELL CLIMATE RESEARCH CENTER conducts science for solutions at the nexus of climate, people and nature. We partner with leaders and communities for just, meaningful impact to address the climate crisis. Our scientists helped to launch the United Nations Framework Convention on Climate Change in 1992, and in 2007, Woodwell scientists shared the Nobel Prize awarded to the Intergovernmental Panel on Climate Change. For 40 years, Woodwell has combined hands-on experience and policy impact to identify and support societal-scale solutions that can be put into immediate action. This includes working with municipalities on the frontlines of the climate crisis.

149 Woods Hole Road, Falmouth, MA 02540 ■ 508-540-9900 ■ [woodwellclimate.org](https://www.woodwellclimate.org)